# Canadian Aerosol Module: A size-segregated simulation of atmospheric aerosol processes for climate and air quality models 1. Module development

S. L. Gong,[1] L. A. Barrie,[2] J.-P. Blanchet,[3] K. von Salzen,[4] U. Lohmann,[5] G. Lesins,[5] L. Spacek,[3] L. M. Zhang,[1] E. Girard,[3] H. Lin,[1] R. Leaitch,[1] H. Leighton,[4] P. Chylek,[5] and P. Huang[1]

Received 14 December 2001; accepted 18 June 2002; published 8 January 2003.

[1] A size-segregated multicomponent aerosol algorithm, the Canadian Aerosol Module (CAM), was developed for use with climate and air quality models. It includes major aerosol processes in the atmosphere: generation, hygroscopic growth, coagulation, nucleation, condensation, dry deposition/sedimentation, below-cloud scavenging, aerosol activation, a cloud module with explicit microphysical processes to treat aerosol-cloud interactions and chemical transformation of sulphur species in clear air and in clouds. The numerical solution was optimized to efficiently solve the complicated size-segregated multicomponent aerosol system and make it feasible to be included in global and regional models. An internal mixture is assumed for all types of aerosols except for soil dust and black carbon which are assumed to be externally mixed close to sources. To test the algorithm, emissions to the atmosphere of anthropogenic and natural aerosols are simulated for two aerosol types: sea salt and sulphate. A comparison was made of two numerical solutions of the aerosol algorithm: process splitting and ordinary differential equation (ODE) solver. It was found that the process-splitting method used for this model is within 15% of the more accurate ODE solution for the total sulphate mass concentration and <1% accurate for sea-salt concentration. Furthermore, it is computationally more than 100 times faster. The sensitivity of the simulated size distributions to the number of size bins was also investigated. The diffusional behavior of each individual process was quantitatively characterized by the difference in the mode radius and standard deviation of a lognormal curve fit of distributions between the approximate solution and the 96-bin reference solution. Both the number and mass size distributions were adequately predicted by a sectional model of 12 bins in many situations in the atmosphere where the sink for condensable matter on existing aerosol surface area is high enough that nucleation of new particles is negligible. Total mass concentration was adequately simulated using lower size resolution of 8 bins. However, to properly resolve nucleation mode size distributions and minimize the numerical diffusion, a sectional model of 18 size bins or greater is needed. The number of size bins is more important in resolving the nucleation mode peaks than in reducing the diffusional behavior of aerosol processes. Application of CAM in a study of the global cycling of sea-salt mass accompanies this paper [*Gong et al.*, 2002]. *INDEX TERMS:* 0305 Atmospheric Composition and Structure: Aerosols and particles (0345, 4801); 3339 Meteorology and Atmospheric Dynamics: Ocean/atmosphere interactions (0312, 4504); 4801 Oceanography: Biological and Chemical: Aerosols (0305); *KEYWORDS:* atmospheric aerosols, sectional, modeling, climate, air quality

**Citation:** Gong, S. L., et al., Canadian Aerosol Module: A size-segregated simulation of atmospheric aerosol processes for climate and air quality models, 1, Module development, *J. Geophys. Res.*, *108*(D1), 4007, doi:10.1029/2001JD002002, 2003.

[1]Meteorological Service of Canada, Downsview, Ontario, Canada.
[2]Environment Division, Atmospheric Research and Environment Program, World Meteorological Organization, Geneva, Switzerland.
[3]Earth Sciences Department, University of Quebec at Montreal, Montreal, Quebec, Canada.
[4]Department of Atmospheric and Oceanic Sciences, McGill University, Montreal, Quebec, Canada.
[5]Atmospheric Science Program, Department of Physics, Dalhousie University, Halifax, Nova Scotia, Canada.


0148-0227/03/2001JD002002

## 1. Introduction

[2] The significance of aerosol particles in the atmosphere has been recognized in two major environmental issues: climate change and human health effects. They influence climate directly by scattering and absorbing solar and terrestrial radiation. Indirectly, they alter cloud droplet size distributions, and thereby the albedo, lifetime of clouds and precipitation. This leads to a change in the energy budget of the atmosphere that ultimately affects climate.

**Table 1.** Examples of Aerosol Schemes in Selected Air Quality and Global Climate Models

| | Model | Aerosol Module | Main References |
|---|---|---|---|
| PM | CIT | Sectional, multicomponents | [*Meng et al.*, 1998] |
| | CMAQ (Models-3) | Modal, multicomponents | [*Binkowski and Shankar*, 1995] |
| | EURAD-MADE | Modal, multicomponents | [*Ackermann et al.*, 1998] |
| | GATOR | Sectional, multicomponents | [*Jacobson*, 1997a] |
| | UAM4-AERO | Sectional, multicomponents | [*Wexler et al.*, 1994] |
| Climate | Harvard CTM | Bulk sulphate, noninteractive | [*Chin et al.*, 1996] |
| | GISS GCM | Size-distributed soil dust, noninteractive | [*Tegen and Fung*, 1994] |
| | ECHAM | Bulk sulphate, BC and OC | [*Lohmann et al.*, 1999] |
| | Grantour | Bulk black carbon and organic carbon, sulphur, noninteractive | [*Erickson et al.*, 1992; *Liousse et al.*, 1996] |
| | GISS GCM II-prime | Bulk sulphate, nitrate and water, noninteractive | [*Adams et al.*, 2001] |
| | MIRAGE | Four multicomponent modes, interactive | [*Ghan et al.*, 2001b] |
| | GATOR | Sectional, multicomponents, noninteractive | [*Jacobson*, 2001] |
| | GOCART | Size-distributed soil dust, noninteractive | [*Ginoux et al.*, 2001] |

The most recent consensus [*Intergovernmental Panel on Climate Change* (*IPCC*), 2001] is that the global mean direct forcing of anthropogenic aerosols is $-0.5$ W m$^{-2}$ with a confidence limit between $-0.2$ to $-0.8$ Wm$^{-2}$ while the indirect forcing is very uncertain. For sulphate aerosols, it is estimated to be between $-1.4$ and $-4.8$ Wm$^{-2}$ [*Ghan et al.*, 2001a; *Lohmann and Feichter*, 1997]. This forcing is opposite in sign and comparable in magnitude to that of anthropogenic greenhouse gases. Thus, a failure to properly deal with the atmospheric aerosols in climate models may result in inaccurate assessments of climate response to future anthropogenic emission scenarios.

[3] The size distribution and chemical composition of the aerosols determine the magnitude of their radiative forcing and their residence time (loading) in the atmosphere [*Koloutsou-Vakakis et al.*, 1998]. Given the loading of a specific aerosol type in the atmosphere, a size distribution is required to calculate the radiative forcing using Mie scattering theory. The importance of aerosol composition is recognized through the interactions of aerosol with solar radiation and with clouds. Sulphate aerosols primarily scatter solar radiation and result in a negative forcing (cooling) while black carbon aerosols primarily absorb the solar radiation and present a positive forcing (warming) to the atmosphere [*Charlson and Heintzenberg*, 1995]. The composition affects cloud formation through the aerosol activation process [*Ghan et al.*, 1995]. Sulphate aerosols readily serve as cloud condensation nuclei (CCN) while pure black carbon particles are much less effective CCN. In assessing the global impact of aerosols, it is important to take into account not only particle size distributions but also the chemical composition associated with anthropogenic components (e.g. sulphates, nitrate, black carbon, organic particles, biomass burning and soil dust from land-surface-modification) and natural components. The latter are from biomass burning [*Penner et al.*, 1992], sea salt [*Gong et al.*, 1997; *Quinn et al.*, 1999], soil dust [*Ginoux et al.*, 2001; *Tegen and Fung*, 1994, 1996], biogenic organic sources and volcanic emissions [*Graf et al.*, 1997]. The absence of natural aerosols in climate models has resulted in a major uncertainty in assessing aerosol forcing to date [*O'Dowd et al.*, 1999].

[4] General circulation models (GCM) are effective tools in addressing the issues of global climate change. The inclusion of interactive aerosol constituents in GCMs to study the climate impact is still at an early stage, especially for size-segregated multicomponent aerosol processes. Individual bulk or size-segregated aerosol types have been incorporated into various GCMs to study the climatic effects [*Adams et al.*, 2001; *Chin et al.*, 1996; *Ghan et al.*, 2001a, 2001b, 2001c; *Ginoux et al.*, 2001; *Liousse et al.*, 1996; *Lohmann et al.*, 1999; *Tegen and Fung*, 1994; *Tegen et al.*, 1997]. The inclusion of an interactive aerosol module in GCMs is the most ideal way to assess the aerosol impact on climate by feeding back both the direct and in-direct aerosol forcing into the GCM dynamical equations. Up to now, there exist very limited number of climate models that include size-distributed, multicomponent and interactive aerosol modules (Table 1). This is another reason why the current assessment of climatic impact of aerosols is subject to large uncertainties and that more work is needed.

[5] The second major environmental impact of aerosols is on human health. Aerosol particles in the submicrometer size range can be inhaled and thus pose certain health hazards. Increases in ambient particle concentrations are associated with an array of adverse health effects [*Brook et al.*, 2002; *Samet et al.*, 2000; *Vedal*, 1997], ranging from respiratory irritation and small decreases in level of lung function, to mortality. Recent study [*Brook et al.*, 2002] has indicated that short-term inhalation of fine particulate air pollution and ozone at concentrations that occur in the urban environment causes acute conduit artery vasoconstriction. Although the exact mechanism by which the aerosol particles interact with human health is not completely understood, it is believed that the aerosol size distribution and chemical composition are the primary factors that determine health impact [*Burnett et al.*, 1997].

[6] Several models have been developed to simulate the size distributions and composition of aerosol particles in urban or regional scale air quality models, e.g. CIT [*Meng et al.*, 1997, 1998], CMAQ (Models-3) [*Binkowski*, 1998; *Binkowski and Shankar*, 1995], EURAD-MADE [*Ackermann et al.*, 1998], GATOR [*Jacobson*, 1994, 1997a, 1997b; *Jacobson et al.*, 1996] and UAM4-AERO [*Wexler et al.*, 1994]. Rigorous thermodynamic models to predict the physical state and composition of inorganic atmospheric aerosol have also been developed [*Nenes et al.*, 1999]. However, these models were designed for application in a specific geographic region (e.g. Los Angeles) and for a short period of time (weeks). For a global climate model, the treatment of aerosols must be numerically efficient and stable for run times of decades.

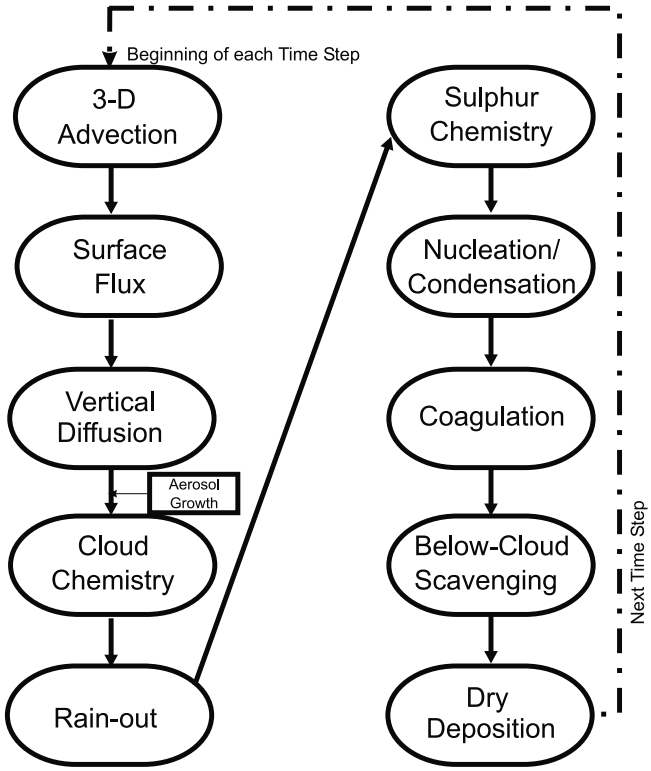


**Figure 1.** The flowchart of process splitting in CAM.

[7] There are two common methods to represent particle size distributions in urban- and regional-scale models: the modal representation and the sectional representation. In the modal approach, each distinct aerosol subpopulation is represented by an analytical modal distribution function [*Binkowski and Shankar*, 1995; *Ghan et al.*, 2001c; *Whitby and McMurry*, 1997]. In the sectional approach, the aerosol size distribution is generally approximated by a set of contiguous, nonoverlapping and discrete size bins. This representation of aerosol size distribution [e.g., *Gong et al.*, 1997; *Jacobson*, 1997a; *Meng et al.*, 1998; *Wexler et al.*, 1994] is employed for its flexibility to treat processes including multicomponent interactions such as coagulation, condensation and chemical processes.

[8] Using the sectional approach, the Canadian Aerosol Module (CAM) was developed to be used in long runs (seasons to years) of global climate models or a chemical transport model (CTM) that yields insight into the role of aerosols in atmospheric environmental issues. It is a size-segregated multicomponent aerosol module including processes such as nucleation, condensation, coagulation, dry deposition, hygroscopic growth, and interaction with clouds as well as wet removal. This paper presents a description of how each process is simulated in CAM and the numerical treatment of the complete CAM aerosol algorithms, using anthropogenic and natural sources of sulphate (SF) and sea-salt (SS) aerosols.

## 2. CAM Aerosol Algorithms

[9] Following the development of CAM using sea-salt aerosols [*Gong et al.*, 1997], the size-distributed multi-component aerosol mass conservation equations are expressed as follows:

$$\frac{\partial \chi_{ip}}{\partial t} = \left.\frac{\partial \chi_{ip}}{\partial t}\right|_{TRANSPORT} + \left.\frac{\partial \chi_{ip}}{\partial t}\right|_{SOURCES} + \left.\frac{\partial \chi_{ip}}{\partial t}\right|_{CLEAR\ AIR} + \left.\frac{\partial \chi_{ip}}{\partial t}\right|_{DRY} + \left.\frac{\partial \chi_{ip}}{\partial t}\right|_{IN-CLOUD} + \left.\frac{\partial \chi_{ip}}{\partial t}\right|_{BELOW-CLOUDS} \quad (1)$$

In equation (1), the rate of change of mixing ratio of dry particle mass constituent $p$ in a size range $i$ has been divided into components (or tendencies) for transport, sources, clear air, dry deposition/sedimentation, in-cloud and below-cloud processes. The sources include surface emission rate of both natural and anthropogenic aerosols. Production of secondary aerosols, i.e. airborne aerosol mass produced by chemical transformation of their precursors together with particle nucleation, condensation and coagulation form the clear air processes. Large scale and subgrid transport of aerosols is carried out by the host model to which CAM is coupled. This is the process indicated in equation (1) by transport tendency which includes the processes of 3-D Advection and Vertical Diffusion/Convection in Figure 1. The following sections describe how other processes are included in equation (1).

### 2.1. Aerosol Properties

[10] The aerosol size spectrum is divided into a number of bins ($N_B$). In this section, the mixing state of various types of aerosols will be defined. Based on the mixing assumptions, the ambient size and density of aerosols in a size bin are evaluated. The optical properties of these aerosols are readily computed once the mixing state, composition and ambient size are determined.

#### 2.1.1. Mixing Scheme

[11] Within a size bin, an internally mixed aerosol is assumed for all types of aerosols except for the freshly emitted (at source grid) insoluble components (BC - black carbon and SD - soil dust) which are assumed to be externally mixed for a fixed amount of time (e.g. one integration time step) in that grid and layer. This essentially assumes that the aging time for insoluble components is constant and limited in space. In a climate model, there is a compromise in parameterization required because aging processes cannot be rigorously simulated due to computational limitations. The number densities of externally mixed components are calculated for every time step in the source grid. This number density is then used in the calculations of aerosol activation and radiative forcing to take the externally mixed aerosol into account, which enables the exclusion of freshly emitted black carbon and soil dust as CCN in our model.

#### 2.1.2. Ambient Aerosol Size

[12] Ambient aerosol size is defined here as the aerodynamic size of aerosol particles in equilibrium with ambient relative humidity. It is calculated from modeled dry size distribution and humidity taking into account the hygroscopic growth of aerosol particles. As aerosol particles grow, the particle density is also changed. To estimate both ambient size and density, assumptions are needed for the growth factors for each type of aerosol. Soluble species grow as relative humidity increase while insoluble components remain unchanged regardless of relative humidity

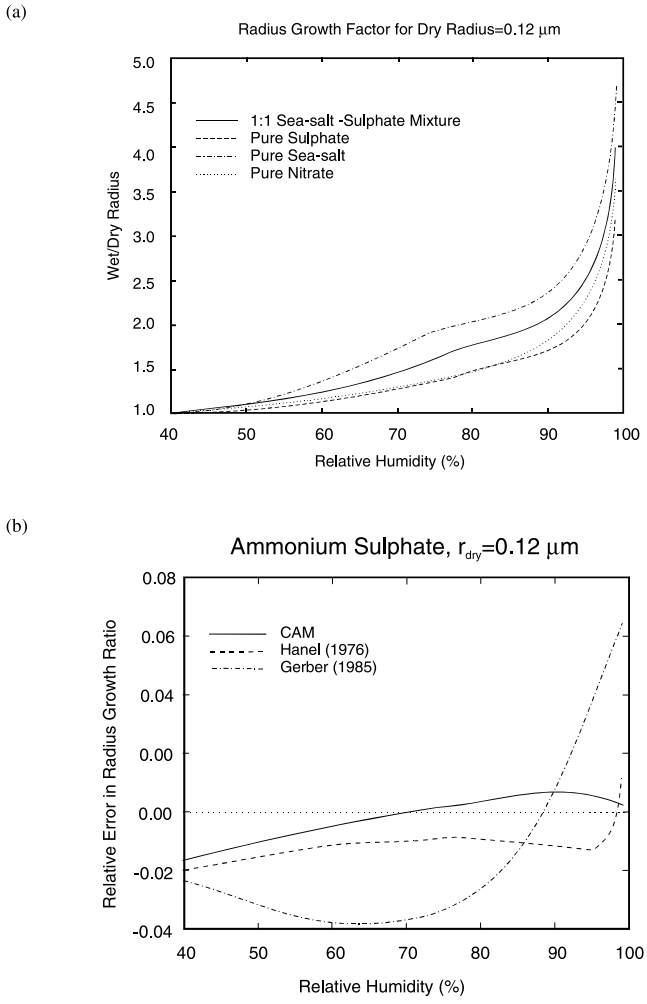


**Figure 2.** (a) Growth factor for one-to-one mixture of sea salt and ammonium sulphate, pure ammonium sulphate, pure sea salt and pure ammonium nitrate; (b) Relative error in the radius growth ratio.

change. The total ambient aerosol mass in a size bin is estimated as:

$$m_{TOT} = m_{BC} + m_{SD} + m_S + m_W \quad (2)$$

where $m_{BC}$ are $m_{SD}$ the mass of black carbon and soil dust respectively, $m_S = m_{SS\ +\ SF\ +\ OC\ +\ NT}$ is the total mass of soluble species (OC for organics and NT for nitrate) and $m_W$ is the water uptake. For each size bin, a mean density of the aerosol particles can be estimated from the particulate composition and water uptake. Assuming a spherical shape for aerosol particles, their size can then be calculated by using $m_{TOT}$ and the density of mixed aerosols. *BC* and *SD* aerosols do not grow with relative humidity, so the process is reduced to the growth of mixed soluble aerosols as a function of relative humidity.

[13] There exist several methods to estimate the water uptake by mixed soluble aerosols [*Cohen et al.*, 1987a, 1987b; *Saxena and Peterson*, 1981]. The so-called ZSR (Zdandovskii-Stokes-Robinson) method [*Sangster et al.*, 1973; *Stokes and Robinson*, 1966] has been used in treating multicomponent aerosol solutions. However, the curvature effect of droplets was not taken into consideration in this approach, which limits its application only to large aerosol droplets. An approach proposed by *Hänel* [1976] is adapted in CAM to treat multicomponent aerosol mixtures that consist of both soluble and insoluble parts. It is assumed that the insoluble component is completely immersed in the solution droplet and that it does not affect the amount of water uptake by the soluble component, is not a surface-active substance and does not engage in a chemical reaction. The equilibrium condition for a solution droplet in moist air is given by the Köhler equation. The numerical treatment of the growth equation and the water activity of each component are given in Appendix A1.

[14] The radius growth factor ( $f_r$) is plotted as a function of the ambient relative humidity at 0°C for the following solutes: one-to-one mixture of sea salt and ammonium sulphate, pure ammonium sulphate, pure sea salt and pure ammonium nitrate (Figure 2a). For all curves the dry aerosol particle has a radius of 0.12 μm. The kinks in the curves between 70 and 80% are the deliquescence points. Below the deliquescence points a linear interpolation to the crystal state is used since the relative humidity history of the particle is normally unknown and efflorescence generally delays the return of a deliquesced aerosol to dryness well below the deliquescence point.

[15] The relative error in $f_r$ with respect to an exact iterative numerical solution of the Köhler equation using measured water activities and solution densities from *Tang and Munkelwitz* [1994] is shown in Figure 2b as a function of the ambient relative humidity for our parameterization and two commonly used parameterizations [*Gerber*, 1985; *Hänel*, 1976] for a pure ammonium sulphate particle with a dry radius of 0.12 μm. The error in our CAM curve is mostly a result of the error in using the density-mixing rule rather than the error in density of an ammonium sulphate aqueous solution.

## 2.2. Clear-Sky Processes

### 2.2.1. Sulphur Chemistry

[16] The reactions in Table 2 are used for calculating sulphur gas transformation rates to condensable $SO_4^{2-}$ in clear skies. Often, in GCM applications the oxidant concentrations are not calculated on-line. The global three-dimensional daily averaged fields of OH, $O_3$, $H_2O_2$ and $NO_3$ from the NCAR MOZART model [*Brasseur et al.*, 1998; *Hauglustaine et al.*, 1998] for one year are imported to CAM. A strong diurnal variation is imposed on mixing ratios of OH and $NO_3$ according to the cosine of solar zenith angle with an average values equal to that imported from MOZART. $O_3$ and $H_2O_2$ are active in cloud chemistry. In the current configuration, four gaseous species, i.e. $H_2S$, DMS, $SO_2$ and $H_2SO_4$, are carried as prognostic variables. For chemical transport model (CTM) applications, the concentrations of highly reactive or condensable species are calculated on-line and used by CAM.

[17] This off-line approach of oxidant chemistry has the advantage of small numerical overhead in a climate model and provides a climatological mean concentration of major oxidants for clear-sky and cloud sulphur chemistry in CAM. However, the off-line approach neglects the strong coupling of $H_2O_2$ and $SO_2$, which can be especially important in the winter NH when photochemical production of $H_2O_2$ is relatively low [*Roelofs et al.*, 1998]. The other problem with the use of off-line chemistry is the mismatch of meteorology

**Table 2.** CAM Chemical Reactions for Sulphur Species

| | Reactions | Rate Coefficient,[a] $cm^3$ $molecule^{-1}$ $s^{-1}$ | Reference[b] |
|---|---|---|---|
| $SO_2$ Production | $DMS + OH \rightarrow SO_2 + \ldots$ | $9.6 \times 10^{-12} \exp(-234/T)$ | 1 |
| | $DMS + OH \rightarrow 0.75\ SO_2 + 0.25MSA + \ldots$ | $\frac{1.7\times10^{-42}\exp(7810/T)[O_2]}{1+5.5\times10^{-31}\exp(7460/T)[O_2]}$ | 1 |
| | $DMS + NO_3 \rightarrow SO_2 + HNO_3$ | $1.9 \times 10^{-13} \exp(500/T)$ | 3 |
| | $H_2S + OH \rightarrow SO_2 + \ldots$ | $6.3 \times 10^{-12} \exp(-80/T)$ | 2 |
| $SO_2$ Oxidation | $SO_2 + OH \rightarrow H_2SO_4 + \ldots$ | $\left\{\frac{k_0(T)[M]}{1+k_0(T)[M]/k_\infty(T)}\right\}0.6^{\left\{1+[\log k_0(T)[M]/k_\infty(T)]^2\right\}^{-1}}$ with $k_0 = 3.0 \times 10^{-31} \times (300/T)^{3.3}$ *and* $k_\infty = 1.5 \times 10^{-12}$ | 2 |

[a] $T$ = temperature (K), $[O_2]$ = $O_2$ density in molecule $cm^{-3}$, [M] = air density in molecule $cm^{-3}$.
[b] References: 1, *Atkinson et al.* [1989]; 2, *DeMore et al.* [1992]; 3, *Pham et al.* [1995].

between the off-line chemistry model and the host model, i.e. precipitation, clouds and radiation. This affects the spatial distribution and availability of the oxidants in case of a nonsynchronized event, and subsequently the precursor distributions and sulphur clear sky and cloud chemistry. *Barrie et al.* [2001] noted this in a comparison of DMS spatial distribution computed by a GCM using both on-line and off-line chemistry. Ultimately as computers become more powerful, on-line chemistry as well as more sophisticated gas-particle equilibrium will be used in model applications. In a regional scale chemical transport model involving CAM with large computational requirements, we are already doing this but limiting it to simulations of short duration.

### 2.2.2. Coagulation

[18] Only binary collisions of particles are considered in CAM. The general coagulation equation can be written as [e.g., *Seinfeld and Pandis*, 1998]:

$$\frac{dN_k}{dt} = \frac{1}{2}\sum_{j=1}^{k-1} K_{j,k-j}N_jN_{k-j} - N_k\sum_{j=1}^{\infty} K_{k,j}N_j \tag{3}$$

where $K_{k,j}$ is the coagulation coefficient between $k$ and $j$ which is calculated from contributions of Brownian, turbulence and gravitational settling movements [*Seinfeld and Pandis*, 1998], and $N_k$ the number concentration in bin $k$. Except for a highly simplified case, there is no analytical solution to equation (3) for practical uses. In CAM, a semi-implicit numerical solution [*Jacobson et al.*, 1994] is used to compute the coagulation rate and intersectional transfer of aerosol particles. This semi-implicit solution conserves volume (mass) with any time step. With the resulting volume change of any size bin due to coagulation, the mass concentration change of each component can be computed accordingly if an internally mixed assumption is made for each size bin.

### 2.2.3. Nucleation and Condensation

[19] Once the condensable species such as $H_2SO_4$(g) are formed in the gas phase by chemical reactions, they participate in two competing processes: nucleation and condensation depending on the particle size, relative humidity and temperature. The rate of change of mass mixing ratio for $H_2SO_4$ vapor due to nucleation can be expressed as:

$$\frac{\partial \chi_{H_2SO_4}}{\partial t} = -C_1 {\chi_{H_2SO_4}}^{C_2} \tag{4}$$

where the constants $C_1$ and $C_2$ are derived from the nucleation parameterization of *Kulmala et al.* [1998] in Appendix A2. The sulphate mass produced by nucleation process is placed in the smallest size bin of a model simulation.

[20] The rate of change of $H_2SO_4$ vapor mass mixing ratio due to condensation can be expressed as

$$\frac{\partial \chi_{H_2SO_4}}{\partial t} = -C_3 \chi_{H_2SO_4} \tag{5}$$

where the constant $C_3$ is given in Appendix A2 from the modified Fuchs-Sutugin equation [*Fuchs and Sutugin*, 1971]. The condensation process does not change the total particle number density but increase the mass of individual particles. As a consequence, particles in bin $i$ will move to bins of larger size. The treatment of condensational growth is handled by the same mechanism as that used by *Jacobson et al.* [1994] to partition the volume of an intermediate particle of two coagulating particles into two model bins. The volume of the condensable species calculated from equation (5) is considered for one of the two colliding particles while the volume of the particle in the condensable bin is considered for the other colliding particle. As dry mass is conserved in every size bin by this mechanism, the growth of aerosol particles from one bin to another may not conserve particle number.

[21] Since nucleation and condensation processes compete in the gaseous phase, the final mass balance equation for $H_2SO_4$ vapor should be written as:

$$\frac{\partial \chi_{H_2SO_4}}{\partial t} = P_{H_2SO_4} - C_3 \chi_{H_2SO_4} - C_1 {\chi_{H_2SO_4}}^{C_2} \tag{6}$$

where $P_{H_2SO_4}$ is the $H_2SO_4$ vapor production rate. There is no analytical solution to equation (6), but it could be solved with an ODE solver. This requires a lengthy iterative procedure at every grid of the 3-D model resulting in extensive use of CPU time. To simplify the solution, equation (6) is approximated as follows:

$$\frac{\partial \chi_{H_2SO_4}}{\partial t} = P_{H_2SO_4} - C_3 \chi_{H_2SO_4} - C_1 \chi_{H_2SO_4} {\chi^0_{H_2SO_4}}^{C_2-1} \tag{7}$$

where $\chi^0_{H_2SO_4}$ is the initial mass mixing ratio of $H_2SO_4$. To ensure that this approximation approaches the real solution as much as possible, a further division of each time step

**Table 3.** Constants for Sulphuric Acid-Water Nucleation Equation

| | 233 K | | 298 K | |
|---|---|---|---|---|
| | 10% RH | 100% RH | 10% RH | 100% RH |
| $C_1$ | $1.7 \times 10^{32}$ | $4.8 \times 10^{16}$ | $3.2 \times 10^{51}$ | $7.6 \times 10^{46}$ |
| $C_2$ | 4.1 | 2.5 | 8.5 | 6.5 |

(e.g. 20 minutes min) into ten sub−time steps was made in our model. Therefore, each $\chi^0_{H_2SO_4}$ was a solution of previous sub−time step. Since equation (7) can be solved analytically, computational time is greatly reduced. Equation (7) has the following solution:

$$\chi_{H_2SO_4}(t) = \frac{e^{-\Omega t}\left[\left(e^{\Omega t}-1\right)P_{H_2SO_4} + \Omega\chi^0_{H_2SO_4}\right]}{\Omega} \qquad (8)$$

where

$$\Omega = C_3 + C_1\chi^{0\ C_2-1}_{H_2SO_4}$$

The tendency of nucleation and condensation is computed from equation (8). For using the kg kg$^{-1}$ as the unit for $\chi_{H_2SO_4}$ the ranges of constants $C_1$ and $C_2$ are listed in Table 3 for various conditions. In addition to temperature and relative humidity, initial $SO_2$ and $H_2SO_4$ (g) concentrations also affect the solution. Figures 3 and 4 show the results of this simplified approach and a rigorous solution of equation (6) with an ODE solver at the same initial conditions. Figure 3 represents the results for an initial mass mixing ratio of 0.001 μg kg$^{-1}$ for $H_2SO_4$. At both 233 K and 298 K, the approximate solutions agree very well with the accurate ODE solver under various conditions. Since the approximate solution places more weight on the initial condition of $H_2SO_4$ (g) concentration for the nucleation process, the agreement is almost perfect (Figure 3a) for low initial $H_2SO_4$ (g) and OH concentrations at 233 K due to the lack of oxidation and nucleation processes. When the initial $H_2SO_4$ (g) mass mixing ratio is increased to 1.0 μg kg$^{-1}$ (Figure 4), nucleation rate increases substantially. At lower temperature (233 K) and higher $SO_2$ (170 nmole mole$^{-1}$), the agreement is also very good since under such conditions the nucleation rate is so large that the vapor $H_2SO_4$ is depleted very rapidly under both solution methods (Figure 4a). Under typical atmospheric conditions listed in Figures 3 and 4, the error is within a factor of 2 to 3 which is acceptable considering the fact that uncertainties in experimental nucleation rates are several orders of magnitudes [*Raes et al.*, 1992].

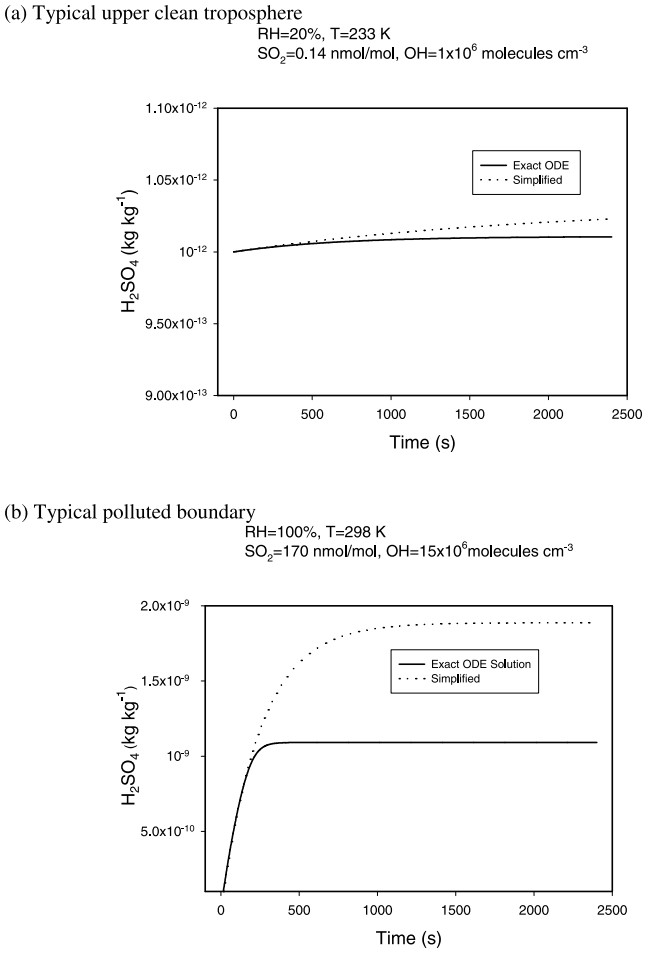


**Figure 3.** Comparisons between an ODE solver and our approximate analytical method for the combined nucleation and condensation equation. The initial $H_2SO_4$ vapor concentration is 0.001 ppbm.

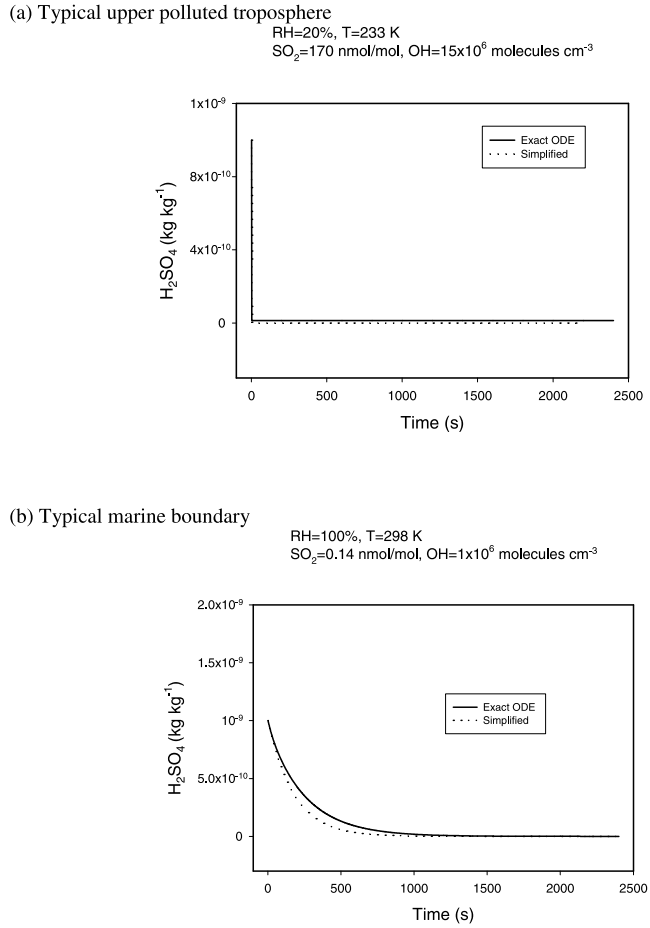


**Figure 4.** Same as Figure 3. The initial $H_2SO_4$ vapor concentration is assumed 1 ppbm.

## 2.3. Dry Deposition/Sedimentation

[22] The dry deposition velocity ($v_d$) of particles as a function of particle size to the ocean's surface has been

**Table 4.** CAM Land Use and Seasonal Categories

| Category | Description |
|---|---|
| | *Land Use Categories (LUC)* |
| 1 | Evergreen-needleleaf trees |
| 2 | Evergreen broadleaf trees |
| 3 | Deciduous needleleaf trees |
| 4 | Deciduous broadleaf trees |
| 5 | Mixed broadleleaf and needleaf trees |
| 6 | Grass |
| 7 | Crops, mixed farming |
| 8 | Desert |
| 9 | Tundra |
| 10 | Shrubs and interrupted woodlands |
| 11 | Wet land with plants |
| 12 | Ice Cap and Glacier |
| 13 | Inland Water |
| 14 | Ocean |
| 15 | Urban |
| | *Seasonal Categories (SC)* |
| 1 | Midsummer with lush vegetation. |
| 2 | Autumn with cropland that has not been harvested. |
| 3 | Late autumn after frost, no snow. |
| 4 | Winter, snow on ground and subfreezing. |
| 5 | Transitional spring with partially green short annuals. |

studied by *Gong et al.* [1997] for sea-salt aerosols. Since dry deposition velocity depends on the ambient size and density of aerosol particles and land surface properties and meteorological conditions, this scheme has been modified to treat multicomponent aerosols and surfaces in CAM [*Zhang et al.*, 2001]. To handle the dry deposition of aerosol gas precursor species, the dry deposition scheme from ADOM [*Padro et al.*, 1991] was incorporated into CAM for $SO_2$ which is the only prognostic gaseous species subject to dry deposition.

[23] Since large scale host models often do not provide sufficiently detailed land use categories (LUC) for gas and particle dry deposition calculations, a high-resolution ($1 \times 1$ km) global land use database from EDC DAAC has been added to CAM. The 15 land use categories and 5 seasons are defined in Table 4. Depending on the grid latitude-longitude and resolution of the mode run, the high-resolution data within the grid square are counted to yield a fractional coverage for each category of the grid. Dry deposition velocity for each available land use within a grid was calculated and the final dry deposition velocity was obtained by averaging the individual dry deposition velocity weighted by its fractional coverage. For particles above the surface layer, settling velocity is calculated as a function of particle size and used to compute the sedimentation tendency of particles aloft.

[24] Figure 5 shows the calculated $v_d$ among various surface types and particle size for seasonal category 1 for particles with a density of 2000 kg $m^{-3}$, a wind speed of 5 m $s^{-1}$ at a height of 20 meters and neutral stratification. $v_d$ values are higher for forests and urban land use than for the other surface types. This is because of the larger roughness lengths and bigger friction velocities for these land use types. Figure 6 shows the variation of $v_d$ with wind speed and particle size. For both land use categories, $v_d$ increases for increasing wind speed for all particle size ranges. A higher wind speed causes higher friction velocity, thus smaller aerodynamic resistance and surface resistance. Particles in the size range of 0.1–2 μm have the

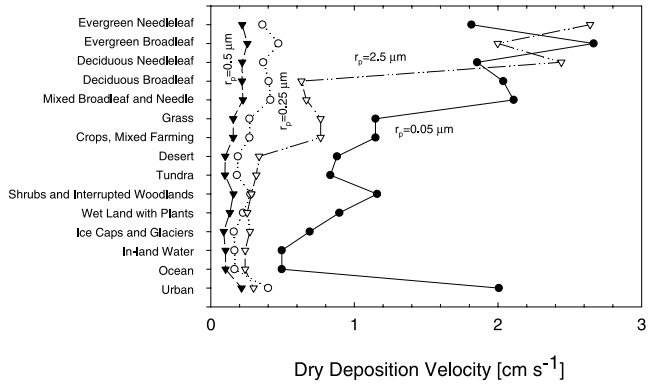


**Figure 5.** Particles dry deposition velocity (reference height 10 m) as a function of size and surface land use category.

smallest $v_d$ value since Brownian diffusion, impaction or interception are least effective in this size range. For this size range, $v_d$ is most sensitive to wind speed changing by an order of magnitude from 2 to 12 m $s^{-1}$. The deposition

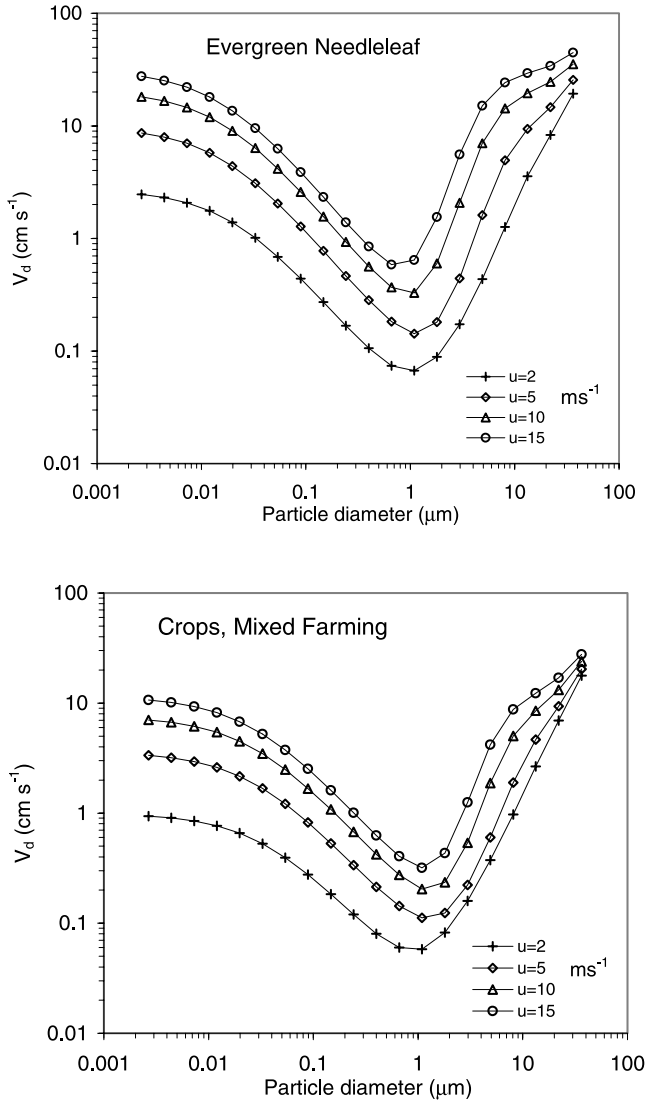


**Figure 6.** Particles dry deposition velocity (reference height 10 m) as a function of size and wind speed.

values shown in Figures 5 and 6 are reasonable when compared to available observational data and other deposition models [*Zhang et al.*, 2001].

### 2.4. Below-Cloud Scavenging

[25] Below-cloud scavenging by precipitation (i.e. rain or snow) is the process of aerosol removal from the atmosphere between cloud base and the ground. The capture of aerosol particles by falling hydrometeors takes place by Brownian and turbulent shear diffusion, inertial impaction, diffusiophoresis, thermophoresis, and electrical effects. Detailed studies of these processes [*Greenfield*, 1957; *Herbert and Beheng*, 1986; *Pilat*, 1975; *Slinn*, 1984] have revealed that there exists a minimum in the collection efficiency of aerosol particles between sizes ranging from 0.5 to 1 μm radius, which is sometimes called the "Greenfield gap". According to *Slinn* [1984], the removal rate of aerosols per unit volume can be written as:

$$\left.\frac{\partial \chi_{ip}}{\partial t}\right|_{BELOW-CLOUDS} = f_{cld} \times \psi(r_i) \times \chi_{ip}(r_i) \qquad (9)$$

where $r_i$ is the averaged actual radius of $i^{th}$ size bin, $f_{cld}$ is the cloud cover fraction, and $\psi$ is the scavenging rate [*Gong et al.*, 1997] that depends on the size of both aerosol and falling hydrometeors.

### 2.5. In-Cloud Processes

[26] In-cloud processes simulated in CAM include: (1) cloud droplet activation, (2) subsequent aerosol-cloud-raindrop interaction and (3) cloud chemistry. The indirect impact of aerosols on climate occurs through these processes. The size distribution and chemical composition of both aerosol and cloud droplets are also modified. The quantities needed by this module are the aerosol number size distribution and composition, concentrations of gas-phase species relevant to cloud chemistry such $O_3$, $H_2O_2$, $SO_2$, $HNO_3$ and $H_2SO_4$, and meteorological conditions especially relevant to clouds such cloud liquid water content, coverage, grid turbulent and gravity wave properties.

#### 2.5.1. Aerosol Activation and Cloud Formation

[27] Clouds are formed in the atmosphere due to the condensational growth of aerosol particles. The conditions for forming clouds depend on aerosol number concentrations, composition and supersaturation. The latter also depends on the vertical motion of the air. The primary function of this module is to use a process parameterization scheme to generate cloud droplet number densities from dry aerosol size distribution and composition given the meteorological conditions in the grid. Approaches to treat the cloud-aerosol interaction range from detailed microphysical models [*Pruppacher and Klett*, 1997] to microphysical based parameterizations [*Ghan et al.*, 1995, 1993] to empirical parameterizations [e.g., *Gultepe and Isaac*, 1996; *Jones et al.*, 1994; *Leaitch et al.*, 1992]. For the anticipated usage of CAM in long term climate and air-quality model simulations, two approaches are adopted: an empirical scheme and a microphysical based parameterization scheme.

[28] For the empirical approach, a formulation from *Jones et al.* [1994] was used to derive cloud droplet number concentration from aerosol number concentrations in a certain size range. The sulphate mass has also been used to calculate the cloud number concentration in climate models [*Lohmann and Roeckner*, 1996]. According to *Jones et al.* [1994], the cloud droplet number ($N_{drop}$) is obtained as:

$$N_{drop} = 3.75 \times 10^8 \left[1 - \exp\left(-2.5 \times 10^{-9} N_a\right)\right] \qquad (10)$$

where $N_a$ is aerosol number concentrations in the size range 0.05–1.50 μm radius in $m^{-3}$ [*Martin et al.*, 1994]. This cloud droplet number density is fed to a cloud module with explicit microphysical processes [*Lohmann and Roeckner*, 1996] to treat the cloud-aerosol interactions. Equation (10) is an empirical relationship based on limited field measurements. Aerosol size distribution, composition and meteorological conditions are not taken into consideration.

[29] A more sophisticated approach is the activation parameterization scheme of *Ghan et al.* [1995, 1993]. Ghan et al.'s parameterization is based on application of Köhler theory to a lognormal aerosol size distribution. To apply this parameterization to a size-segregated multiple type aerosol activation scheme, the aerosol distribution has to be fitted with a single or bimodal lognormal distribution and the vertical velocity in the grid is required. Further research is being carried out to implement this parameterization into CAM.

#### 2.5.2. Aerosol and Precipitation

[30] The interaction between aerosols and clouds in CAM concentrates on the processes that affect aerosol distributions: precipitation formation and scavenging of aerosol particles. Precipitation formation is related to the cloud droplet number concentration in addition to the liquid water content [*Beheng*, 1994]. The precipitation process transfers aerosol mass in cloud droplets into precipitation. According to *Giorgi and Chameides* [1986], the rainout removal tendency is expressed as:

$$\left.\frac{\partial \chi_{ip}}{\partial t}\right|_{IN-CLOUD} = -\lambda \times \chi_{ip}(r_i) \qquad (11)$$

where $\lambda$ is the local removal frequency ($s^{-1}$) which is calculated in terms of the local water vapor condensation (and precipitation) rate $p_r$ (kg $m^{-3} s^{-1}$) [*Giorgi and Chameides*, 1986]. When precipitation evaporates in a layer, the percentage of aerosol mass transferred from the precipitation phase to the cloud or dry aerosol phase is assumed equal to the ratio of the evaporation rate to precipitation rate in that layer.

#### 2.5.3. Cloud Chemistry

[31] The CAM-parameterization of in-cloud production of sulphate takes into account oxidation by hydrogen peroxide and ozone in stratiform and convective clouds [*von Salzen et al.*, 2000]. The sulphur transport and chemistry in convective clouds is based on a simplified version of the plume ensemble concept proposed by *Arakawa and Schubert* [1974]. The simplified version has been developed and successfully tested by *Zhang and McFarlane* [1995] to study deep convection with the CCC GCM.

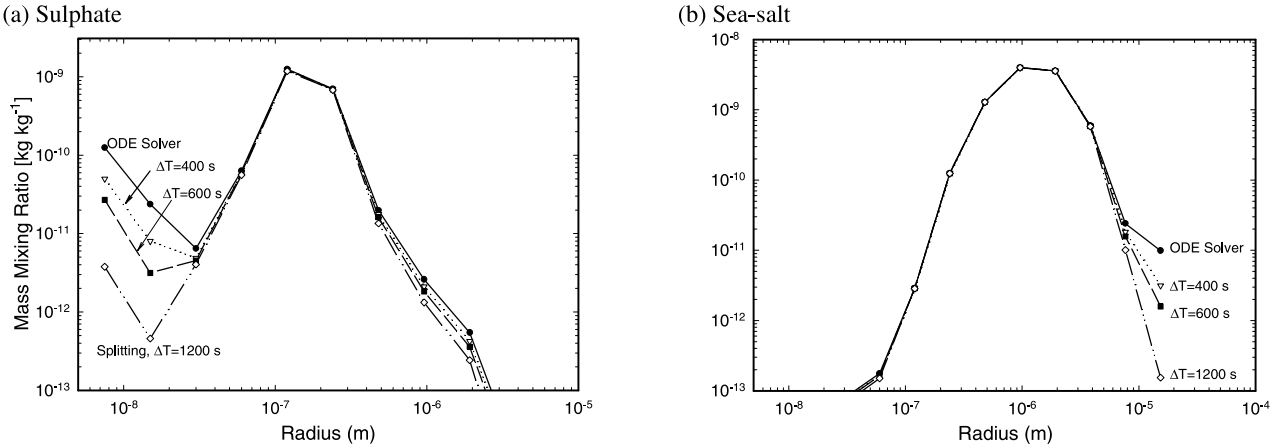


**Figure 7.** The impact of integration time step on the accuracy of CAM solution for sulphate and sea-salt compared using a process-splitting method against an ODE solver solution.

[32] Since it is not possible to include the $H_2O_2$ cycle in CAM due to computing time restrictions, a simple parameterization of the production of $H_2O_2$ from gas phase reactions is applied:

$$\left.\frac{\partial \chi_{H_2O_2}}{\partial t}\right|_{prod} = -\tau^{-1}\left(\chi_{H_2O_2} - \chi^{b}_{H_2O_2}\right) \qquad (12)$$

In GCM applications, the prescribed background concentration $\chi^{b}_{H_2O_4}$ is from a simulation with the MOZART model [*Brasseur et al.*, 1998]. The timescale $\tau$ has a value of 36 h, which is of the order of timescales for observed gas phase production rates in the free troposphere [*Tremmel et al.*, 1993]. The parameterization is applied at every grid point and tends to restore the $H_2O_2$ concentrations after in-cloud depletion of $H_2O_2$ to the prescribed background values.

[33] It should be pointed out that the current parameterization is applied to the bulk cloud phase. The sulphate mass produced by the scheme in clouds is over the activated aerosol spectrum, i.e. cloud droplets [*von Salzen et al.*, 2000]. Since the oxidation chemistry of sulphur species depends on droplet pH, size-dependent chemistry may yield more realistic results. However, the resolution of the model and the simple parameterization of clouds by the explicit scheme do not warrant more detail at this time.

## 3. Numerical Treatments and Model Performance

### 3.1. Integration Method

[34] The aerosol algorithm described in section 2 forms a set of ordinary differential equations and can be solved in two ways: an ODE solver and a process-splitting technique. A solution by an ODE solver is more accurate than that by the process-splitting method but is much more expensive computationally. For a long-term global climate model simulation it is impractical to use an ODE solver even with most supercomputers.

[35] A process-splitting technique is used to solve equation (1). Figure 1 shows a flowchart of the sequence in which processes are solved. The process-splitting method has been widely used in large-scale atmospheric models involving photochemistry and other processes. Convergence and the accuracy depend on the order of the processes split and the time step used. In order to test the performance of the process-splitting scheme developed in this study, a rigorous solution of CAM equations was produced with an SMVGEAR ODE solver and used as a benchmark against which process-splitting approximations could be compared.

[36] The comparisons were made between splitting and SMVGEAR solutions as a function of particle size at integration time steps of 400, 600 and 1200 s for both sulphate and sea-salt using 12-size bin configuration (Figure 7). Both methods started with the same initial conditions and surface fluxes. After 6 hours of integration, differences appear whose magnitude depends on the splitting integration time step. For both sea salt and sulphate, the splitting solutions approach the accurate solution as the integration time step is reduced. The difference also depends on particle size. For sulphate (Figure 7a), the discrepancy is large for $r < 0.03$ μm where nucleation tendency is high and for $r > 0.5$ μm where dry deposition tendency is increasing (Figure 3). There exists a very small discrepancy for sea-salt aerosol for $r > 6$ μm due to the large dry deposition and settling velocity (Figure 7b). Nevertheless, the splitting method predicts a similar peak concentration and mode width with the ODE solver. From the analysis, we conclude that the CAM algorithm solved by the process-splitting method slightly underestimates the aerosol mass concentrations for both sea-salt and sulphate. Depending on the integration time step, the average relative difference of total sulphate aerosol mass over the whole size spectrum ranges from 6 to 15%. The relative difference is also dependent on the magnitude of initial sulphate mass concentration when oxidant and $SO_2$ concentrations are fixed. An increase in initial concentration results in a better performance.

[37] The advantage of the process-splitting method is the substantial CPU time reduction compared with the fully coupled solution. Table 5 summarizes the CPU usages for coupled and process-splitting methods at various time steps. For an integration time step of 1200 s, the CPU usage ratio of coupled ODE solution to the process-splitting solution is

**Table 5.** CPU Usages of Coupled ODE Solution and Process-Splitting Methods

| | Coupled ODE | Process Splitting | | |
|---|---|---|---|---|
| | | 400 s | 600 s | 1200 s |
| CPU (s) | 15.2 | 0.18 | 0.13 | 0.059 |
| Ratio | 1 | 84 | 117 | 258 |

about 258 times. For a large-scale climate or air-quality modeling system, this accounts for a tremendous saving of CPU time.

[38] The order of the process split influences the results only slightly. For sea-salt aerosols, the difference due to the splitting order is insignificant while for sulphate the difference is noticable but small in the submicron size range. The total sulphate mass concentration difference among various orders of process splitting is within 7%.

### 3.2. Impact of Particle Size Bin Numbers

[39] Using the splitting method described above, the sensitivity of the evolution of an initial size distribution in CAM to the number of size bins was investigated. The aim of this sensitivity test was to find out those conditions under which a model of limited number of size bins adequately predicts aerosol number or mass size distributions. The initial mass size distributions were chosen to represent the typical sulphate and sea-salt concentrations in the atmosphere. The mass mean radii and standard deviations for sulphate and sea-salt are 0.148 μm, 1.33 and 1.36 μm, 1.82 respectively. For a radius spectrum from 0.005 μm to 20.48 μm and a size bin width with $r_{i2}/r_{i1} = 2$ ($r_{i2}$ and $r_{i1}$ are the up and lower radius bounds of size bin $i$), the initial size segregated distributions for various size bin resolutions were shown in Figure 8 by solid lines. It is noted that due to the sectional representation, the initial distribution shape for each size bin configuration is slightly different (Table 6).

[40] The performance of the sectional model for three individual processes (coagulation, deposition and nucleation/condensation) and one all-inclusive simulation was tested for the size bin number of 8, 12, 18 and 96. Figure 8 summarizes the results using various size bin configurations after 6 hours of simulation. Two immediate conclusions can be drawn from Figure 8: (1) deposition processes (Figures 8a (2) and 8b (2)) have little numerical diffusion regardless of size bin numbers and aerosol types and (2) due to the large particle size, sea-salt has very little numerical diffusion for coagulation (Figure 8b (1)). Therefore, a 12-size bin configuration is adequate to simulate sea-salt aerosol mass concentrations.

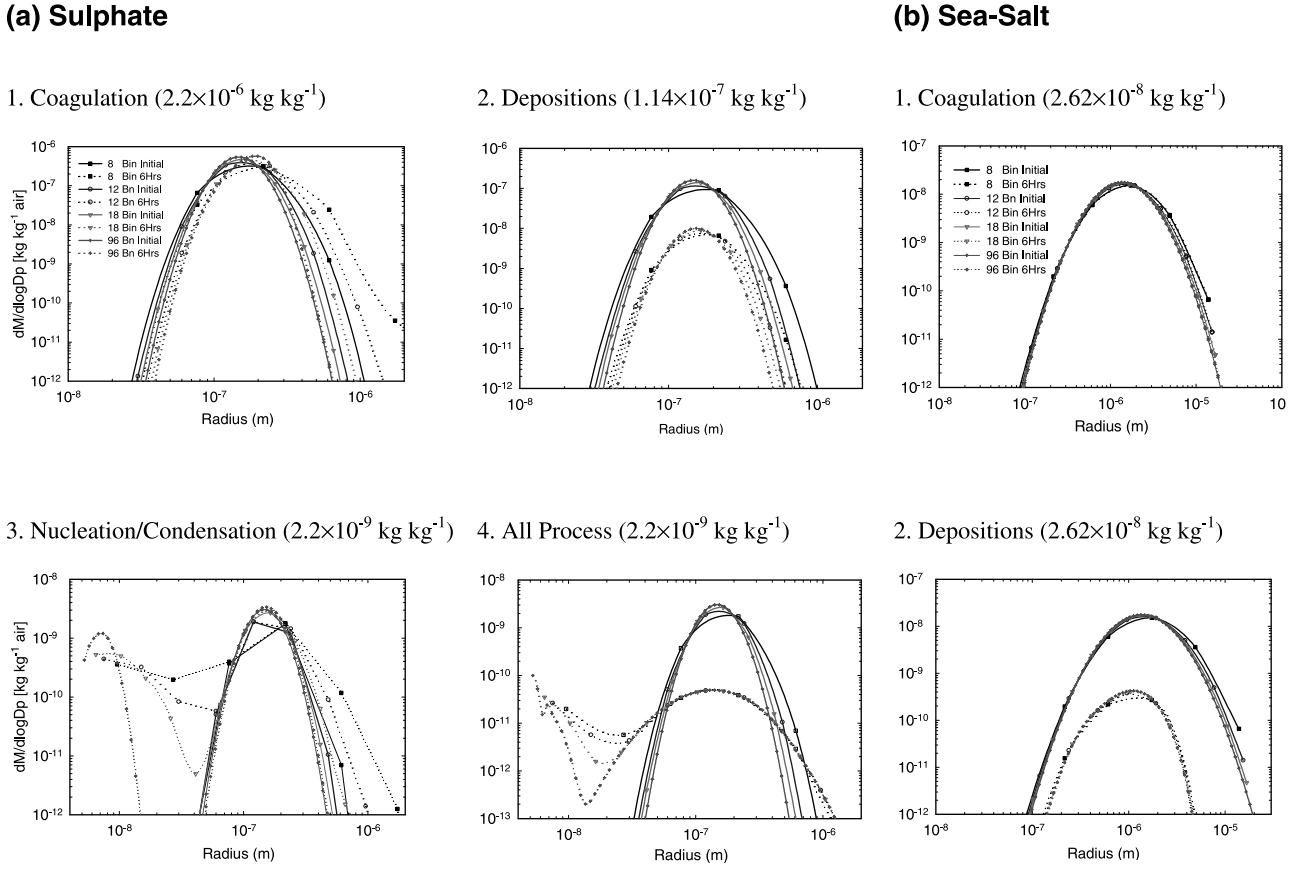


**Figure 8.** Impacts of sectional model resolution on the mass concentrations for three individual process and all-inclusive simulations: (a) sulphate and (b) sea-salt. The solid curves in each plot represent the initial size distributions for different number of size bins. The initial concentration of each test is given in the bracket. In nucleation/condensation case, $H_2S = 1.2 \times 10^{-10}$ kg kg$^{-1}$, DMS = $3.18 \times 10^{-11}$ kg kg$^{-1}$, $SO_2 = 1.4 \times 10^{-8}$ kg kg$^{-1}$ with OH = $1.78 \times 10^{-14}$ cm$^3$ cm$^{-3}$.

**Table 6.** Mass Mean Radii ($r$) and Standard Deviation ($\sigma$) of Lognormal Fitted Mass Size Distributions for Initial and Processed Sulphate and Sea-Salt Aerosols at Various Size Bin Resolutions[a]

| Bins | Initial | | Coagulation | | | | Depositions | | | | Nucleation/Condensation | | | |
|---|---|---|---|---|---|---|---|---|---|---|---|---|---|---|
| | $\sigma_0$ | $r_0$ | $\sigma_1$ | $r_1$ | $\frac{\delta\sigma}{\sigma_0}$ | $\frac{\delta r}{r_0}$ | $\sigma_2$ | $r_2$ | $\frac{\delta\sigma}{\sigma_0}$ | $\frac{\delta r}{r_0}$ | $\sigma_3$ | $r_3$ | $\frac{\delta\sigma}{\sigma_0}$ | $\frac{\delta r}{r_0}$ |
| *Sulphate* | | | | | | | | | | | | | | |
| 8 | 1.48 | 0.162 | 1.60 | 0.210 | **8.11** | **29.8** | 1.45 | 0.16 | **−2.03** | **3.22** | 1.66 | 0.187 | **12.2** | **15.4** |
| 12 | 1.41 | 0.158 | 1.48 | 0.184 | **4.68** | **16.9** | 1.40 | 0.165 | **−0.71** | **5.02** | 1.46 | 0.161 | **3.55** | **2.10** |
| 18 | 1.37 | 0.151 | 1.38 | 0.180 | **1.08** | **19.1** | 1.37 | 0.158 | **−.073** | **4.13** | 1.40 | 0.157 | **2.19** | **3.73** |
| 96 | 1.33 | 0.148 | 1.31 | 0.185 | **−1.50** | **25.2** | 1.33 | 0.153 | **−.075** | **3.56** | 1.33 | 0.151 | **0.00** | **2.55** |
| *Sea Salt* | | | | | | | | | | | | | | |
| 8 | 1.96 | 1.55 | 1.97 | 1.56 | **0.51** | **0.582** | 1.77 | 1.10 | **−9.69** | **−28.9** | | | | |
| 12 | 1.88 | 1.44 | 1.88 | 1.45 | **0.00** | **0.555** | 1.76 | 1.04 | **−6.38** | **−28.0** | | | | |
| 18 | 1.85 | 1.40 | 1.85 | 1.40 | **0.00** | **0.573** | 1.73 | 1.04 | **−6.49** | **−25.6** | | | | |
| 96 | 1.82 | 1.36 | 1.82 | 1.37 | **0.00** | **0.588** | 1.73 | 1.03 | **−4.95** | **−24.3** | | | | |

[a]Here $\frac{\delta\sigma}{\sigma_0}$ and $\frac{\delta r}{r_0}$ are in percent, and $r$ is in μm. Nucleation/condensation fitting was done only for the accumulation mode distributions.

[41] Depending on the number of size bins, the sectional approach has a certain degree of numerical diffusion for the sulphate nucleation/condensation and coagulation processes. For the coagulation process, this diffusional behavior (Figure 8a (1)) has already been discussed by *Jacobson et al.* [1994]. For a low-resolution sectional model (e.g. bin = 8), this diffusion is substantial. We also found out that the diffusional behavior for coagulation process depends on not only the size bin numbers but also the initial concentrations. When total initial mass concentration decreases, the numerical diffusion tends to become weaker due to the decreases in coagulation tendency. Little numerical diffusion was found when the initial mass concentration was reduced from $2.2 \times 10^{-6}$ kg kg$^{-1}$ (Figure 8a (1)) to $2.2 \times 10^{-9}$ kg kg$^{-1}$. Given the exceptionally high initial concentration for coagulation, the estimate of the numerical diffusion in Figure 8a (1) is an upper limit.

[42] In order to quantitatively characterize the numerical diffusion for a given size bin resolution, the initial and after 6 hours size distributions were fitted into a lognormal distribution with respective mass mean radius ($\bar{r}$) and standard deviations ($\sigma$). The relative changes in $\bar{r}$ and $\sigma\left(\frac{\delta r}{r_0}\text{ and }\frac{\delta\sigma}{\sigma_0}\right)$ reflect the degrees of numerical diffusion compared to the results of 96 size bins which are assumed to have little diffusion. Table 6 lists the changes of $\bar{r}$ and $\sigma$ for different size bin resolutions with three individual processes for sulphate, and coagulation and deposition processes for sea-salt. It should be pointed out that this kind of fitting is associated with some uncertainties but the general trends from the analysis are conclusive.

[43] For the nucleation/condensation processes, Figure 8a (3) indicates that particle size - resolution impacts not only the numerical diffusion but also the resolution of sulphate peaks below r < 0.05 μm. For a bin number of 96 or 18, a distinct minimum for mass distribution is simulated around r = 0.02 μm or r = 0.04 μm, which yields a nice bimodal distributions. Bin numbers of 8 or 12 hardly resolve this minimum. This indicates that when the nucleation mode peaks need to be resolved in a major nucleation event, a size bin number of at least 18 should be used. For the accumulation mode peak around r = 0.1 μm in Figure 8a (3), $\frac{\delta\sigma}{\sigma_0}$ and $\frac{\delta r}{r_0}$ for 96 bins are 0.00 and 2.55%, respectively, which implies that there exists no change in width of the distribution but 2.55% shifts in radius due to condensational growth. Except for bin = 8 which has large changes in both $\frac{\delta\sigma}{\sigma_0}$ and $\frac{\delta r}{r_0}$, bin numbers of 12 and 18 have similar changes in $\frac{\delta r}{r_0}$ (2.1% and 3.73%) compared to bin = 96 but somewhat large changes in $\frac{\delta\sigma}{\sigma_0}$, indicating that models with bin numbers of 12 and 18 can predict a reasonable peak concentration in the accumulation mode but with some numerical diffusions. It is obvious that the number of size bins used in simulating the nucleation/condensation processes is more critical in resolving the nucleation mode peaks than in reducing the numerical diffusion by coagulation and condensation.

[44] Figure 8a (4) illustrates a typical situation including all processes in anthropogenic emission regions where the primary particles are released with a size distribution. Apparently, the impact of the flux depends on the magnitude and the shape of the distribution. When the primary particle flux and the secondary gas-to-particle conversion contribute similarly to the concentrations in Figure 8a (4), the sensitivity to size bin number is much less for all size ranges important in radiative forcing (r > 0.05 μm). However, for bin numbers of 8 and 12, the distinct minimum at r = 0.02 μm is still not well resolved. The less numerical diffusion in this case was also due to the deposition processes which reduced the overall mass concentrations and consequently the tendency for coagulation.

[45] To further investigate the impact of sectional model resolution, the total sulphate aerosol number and mass concentrations simulated for 6 hours by size bin numbers of 8, 12, 18, 36 and 96 were shown in Figure 9 for coagulation, deposition, nucleation/condensation and all-inclusive simulations. The relative difference (RD) in number and mass against results from 96 bins was used as a diagnostic parameter for the model performance and shown on the top panel of each plot in Figure 9. For coagulation process (Figures 9a (1) and 9b (1)), there is a slight decrease in total number and no change in total mass, which is characteristic of coagulation process. The RDs in number concentration range from 5 to 15% but almost 0% for RDs in mass concentration, indicating some degree of the numerical diffusion for total number concentrations. For the deposition processes, both number and mass concentration agree nicely with each other among various bins after 6-hour simulations. The RDs for both number and mass are below 20% except for bin 8 where the differences are as high as 60% (Figures 9a (2) and 9b (2)). This is an

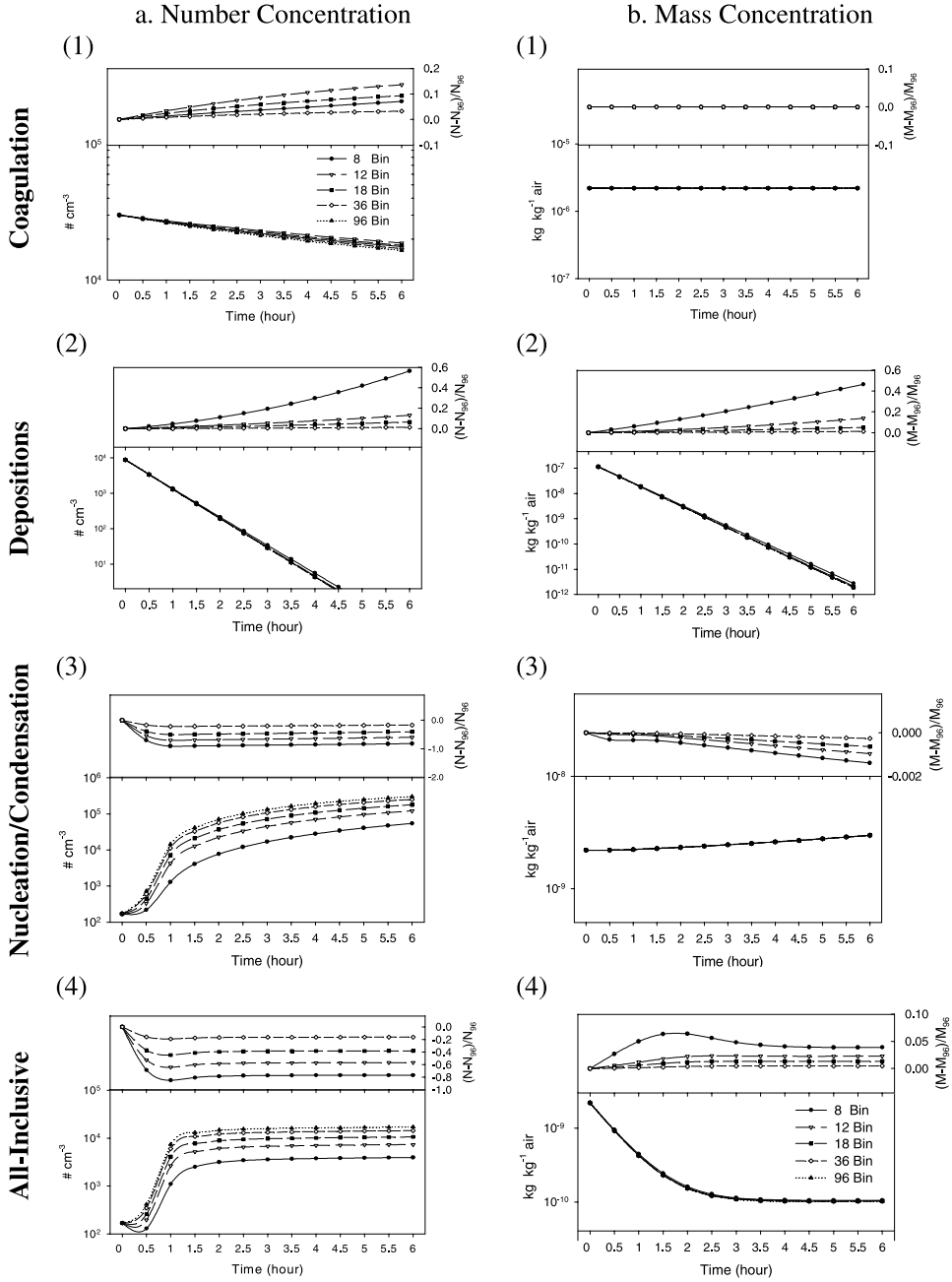


**Figure 9.** Impacts of sectional model resolution on the total sulphate number and mass concentrations for three individual process and all-inclusive simulations as a function of time. Top panel of each plot shows the relative difference of number and mass compared with 96 bin results.

indication that less size bin number models can cause uncertainties in deposition calculations if running alone for a long period of time (e.g. 6 hours) and ending in very low concentrations. The total number concentration due to nucleation/condensation process is very sensitive to the size bin resolution. For bin number of 8, the underestimate in total number concentration could reach 90% (Figure 9a (3)). However, the RDs for mass concentration are close to zero (Figure 9b (3)). For all-inclusive simulation, the number concentration is sensitive to the number of size bins and general underestimates are obtained with less size bins (Figure 9a (4)) while all size bins yield a very close total mass concentration (Figure 9b (4)).

[46] The choice of size bin number in a specific application depends on the objective of the model simulation and atmospheric conditions. For an application where the total mass is the main objective, such as $PM_{2.5}$ and $PM_{10}$ in an air-quality modeling system, a sectional model of 8 size bins may be sufficient to obtain a reasonable answer. However, for an application where the number and mass size distributions are the major concerns such as aerosol radiative forcing and aerosol-cloud interactions in a climate model in the free troposphere, 12 size bins are barely the minimum configuration to properly resolve the size distributions. Thus, a compromise is always involved between model performance and computational time. Hybrid models with

variable bin number depending on location in the atmosphere may be one practical compromise.

## 4. Summary and Conclusions

[47] A size-segregated multicomponent aerosol module has been developed to be incorporated into climate and air-quality models. The module treats all the atmospheric processes as a function of particle size with a sectional representation of the size distribution. The aerosols are assumed to be internally mixed.

[48] The hygroscopic growth of mixed aerosols is calculated with a mixing rule for soluble components and the black carbon and soil dust are assumed to be hydrophobic. The dry deposition velocity of both particles and gases is averaged over the fractional contributions of 15 land use categories in a grid. The results are comparable with other investigations of both modeling and observational results.

[49] The inclusion of an explicit cloud module in CAM establishes the linkage between the aerosol concentration and the cloud/precipitation properties and make it possible for the future assessment of in-direct impact of aerosols on climate. For sulphate aerosols, an on-line sulphur chemistry for both clear sky and cloud droplets using the off-line chemical concentrations of OH, $O_3$, $H_2O_2$, $NO_3$ and $NH_3$ is included in the module. The sulphur chemistry for stratiform and convective clouds is treated separately.

[50] A simplified parameterization of sulphate aerosol nucleation and condensation is numerically efficient and reasonably accurate compared to a coupled ODE solution under various conditions. Under the worst scenario, the difference between a rigorous solution and the simplified one is a factor of 3. This is acceptable considering the fact that the nucleation is subject to an uncertainty of several magnitudes and that this factor of 3 is reduced during atmospheric averaging related to advection and mixing.

[51] The complete CAM algorithm was solved with a process-splitting method. A comparison with a coupled ODE solver solution indicates that process-splitting solution is reasonably matches the ODE solutions over the whole size spectrum with some minor discrepancy for sulphate aerosols in the submicron size ranges and for sea salt in the supermicron size ranges. However, the reduction in CPU time usage is more than 100 times. An integration time step of 400 s to 1200 s can be used with reasonable accuracy.

[52] The number of size bins used in a sectional particle size representation is very important to obtain a reasonable particle size distributions for both number and mass concentrations due to the nature of numerical diffusions of the sectional approach. Use of a smaller size bin number, e.g. <12, could result in smoothing a distinct peak which would be resolved if a larger size bins are used. Because of diffusion, models with fewer size bins tend to underestimate the particle number concentrations. The impact of size bin configurations on the total mass concentrations is not as large as on the number concentrations. A size bin number of 12 is the minimum configuration if a meaningful size distribution is to be simulated. It is found that the number of size bins used in simulating the nucleation/condensation processes is more critical in resolving the nucleation mode peaks than in reducing the numerical diffusion by condensation growth.

[53] This model lays the foundation for assessment of the global cycles of various aerosols beginning with a companion paper on sea-salt in the Canadian GCM [*Gong et al.*, 2002]. Subsequent investigation of sea-salt interactions with sulphates in marine area as well as sea-salt-soil dust-anthropogenic aerosol effects downwind of Asia in the North Pacific will follow. As more powerful computers are available and numerical overhead is reduced, more accurate aerosol climate feedback assessments will naturally follow.

## Appendix A

### A.1. Solution of Hygroscopic Growth Equation of Mixed Aerosols

[54] The equilibrium condition for a solution droplet in moist air is given by the Köhler equation:

$$RH = a_w \exp\left(\frac{2\sigma}{\rho_w R_w T r_d f_r}\right) = a_w \exp\left(\frac{A'}{f_r}\right), \qquad \text{(A1)}$$

where $f_r = r/r_d$ is the radius ratio, $r_d$ is the dry aerosol radius, $r$ is the final equilibrium aerosol radius, $RH$ is the relative humidity with respect to water, $\sigma$ is the surface tension between the solution droplet and air, $R_w$ is the gas constant for water vapor, $T$ is the temperature, $\rho_w$ is the density of water and

$$A' = \frac{2\sigma}{\rho_w R_w T r_d}$$

The exponential form for the water activity is used:

$$a_w = \exp\left(-\overline{\Phi}\overline{\nu}\frac{n_s}{n_w}\right) = \exp\left(-\overline{\Phi}\overline{\nu}\frac{M_w}{\overline{M}_s}\frac{m_s}{m_w}\right), \qquad \text{(A2)}$$

where $\overline{\Phi}$ is the empirically determined osmotic coefficient for the mixture, $n_w$ and $n_s$ are the number of moles for water and solute, respectively, $m_w$ and $m_s$ are the masses of water and solute, respectively, $M_w$ is the molecular weight of water and is $\overline{M}_s$ the average molecular weight of the solute mixture. The average molar number of ions dissociated by one mole of dry solute mixture is:

$$\overline{\nu} = \sum_{i=1}^{N_s} \nu_i \frac{n_{si}}{n_s} = \sum_{i=1}^{N_s} \nu_i \frac{m_{si}}{m_s}\frac{\overline{M}_s}{M_i} = \frac{\overline{M}_s}{f_{msd}} \sum_{i=1}^{N_s} \frac{\nu_i f_{mi}}{M_i}, \qquad \text{(A3)}$$

where $\nu_i$ is the number of ions liberated from each of the $N_s$ solute molecule types, $f_{mi}$ is the mass fraction of the $i^{th}$ solute component with respect to the total dry aerosol and $f_{msd}$ is the mass fraction of all the solute with respect to the total dry aerosol. The average practical osmotic coefficient of the solute mixture is assumed to be:

$$\overline{\Phi} = \frac{1}{\overline{\nu}} \sum_{i=1}^{N_s} \nu_i \Phi_i \frac{n_{si}}{n_s} = \frac{1}{\overline{\nu}} \sum_{i=1}^{N_s} \nu_i \Phi_i \frac{\overline{M}_s}{M_i}\frac{m_{si}}{m_s} = \frac{\overline{M}_s}{\overline{\nu} f_{msd}} \sum_{i=1}^{N_s} \nu_i \Phi_i \frac{f_{mi}}{M_i}. \qquad \text{(A4)}$$

Note that the values $\Phi_i$ for must be evaluated at the same water activity, $a_w$, for each component of the mixture. With this mixing rule the total water adsorbed onto a mixture of

solutes is equal to the sum of the water adsorbed onto each solute component of the mixture evaluated at the same water activity. This mixing rule is identical to the ZSR mixing rule that is quoted in the chemical literature.

[55] In the expression for $a_w$ (Equation (A2)) we can write

$$\frac{m_s}{m_w} = \frac{f_{msd} m_d}{m_w} = \frac{f_{msd}\rho_d V_d}{\rho_w V_w} = \frac{f_{msd}\rho_d V_d}{\rho_w (V - V_d)} = \frac{f_{msd}\rho_d r_d^3}{\rho_w (r^3 - r_d^3)} = \frac{f_{msd}\rho_d}{\rho_w (f_r^3 - 1)}, \tag{A5}$$

where $V$ is the volume of the solution droplet, $V_d$ is the dry volume, $V_w$ is the volume of water uptake and $m_d$ is the total dry aerosol mass. It is assumed that the dry aerosol is spherical and that the solution volume is equal to the sum of the dry solute volume and the water uptake volume. This allows the average dry density of the aerosol mixture to be computed:

$$\rho_d = \frac{m_d}{V_d} \frac{m_d}{\sum_{i=1}^{N_d} V_i} = \frac{m_d}{\sum_{i=1}^{N_d} \frac{m_i}{\rho_i}} = \left[ \sum_{i=1}^{N_d} \frac{f_{mi}}{\rho_i} \right]^{-1}, \tag{A6}$$

where $N_d$ are the total number of aerosol components, both soluble and insoluble. The Köhler equation (A1) becomes:

$$\ln RH = \frac{A'}{f_r} - \overline{\nu}\overline{\Phi} \frac{M_w}{\overline{M}_s} \frac{\rho_d}{\rho_w} \frac{f_{msd}}{f_r^3 - 1} = \frac{A'}{f_r} - \frac{B}{f_r^3 - 1}, \tag{A7}$$

where

$$B = \overline{\nu}\overline{\Phi} f_{msd} \frac{M_w}{\overline{M}_s} \frac{\rho_d}{\rho_w}, \tag{A8}$$

We wish to solve (A7) for $f_r$. The $\Phi_i$ that is needed for determining $B$ is obtained from the measurements [*Tang*, 1996; *Tang and Munkelwitz*, 1994; *Tang et al.*, 1997]. They are converted to the following polynomial curve fit as a function of water activity:

$$\Phi_i(a_w) = \sum_{n=1}^{N_\varphi} \varphi_{i,n} a_w^n.$$

Now solving for $f_r$ using Equations (A1) and (A5)

$$f_r = \left[ 1 - \frac{\overline{\nu}\overline{\Phi} M_w \rho_d f_{msd}}{\overline{M}_s \rho_w \ln a_w} \right]^{1/3}. \tag{A9}$$

This value for $f_r$ is then used to provide the next estimate for $a_w$ (Equation (A2)):

$$a_w = RH \exp\left( \frac{-A'}{f_r} \right). \tag{A10}$$

The updated value for $a_w$ is then used in (A9). The above procedure need be repeated only one more time to obtain better than 1% accuracy for $f_r$. Errors can be reduced to less than 0.1% if one further iteration is performed. A slight refinement in the value for $f_r$ is computed if the relative humidity is greater than 98% since the final equilibrium radius is a very rapidly increasing function in this region.

### A.2. Nucleation and Condensation Equation

[56] The nucleation rate, molecule cm$^{-3}$ s$^{-1}$, of vapor sulphuric acid is expressed as a function of vapor sulphuric acid concentration ($N_a$, molecule cm$^{-3}$), temperature (T) and relative humidity (*RH*) [*Kulmala et al.*, 1998]:

$$J_{nucl} = \exp(\theta) \tag{A11}$$

with

$$\begin{aligned} \theta &= AN_{sulf} + BX_{al} + C \\ A &= 25.1289 - 4890.8/T - 1743.3/T - 2.2479\delta RH \\ B &= 7643.4/T - 1.9712\delta/RH \\ C &= -1743.3/T \\ N_{sulf} &= \ln(N_a/N_{a,c}) \\ \delta &= T/273.15 \end{aligned}$$

where $N_{a,c}$ is the vapor sulphuric acid concentration needed to produce the nucleation rate of 1 cm$^{-3}$ s$^{-1}$ given as:

$$N_{a,c} = \exp(-14.5125 + 0.1335T - 10.5462RH + 1958.4RH/T) \tag{A12}$$

and $X_{al}$ is the $H_2SO_4$ mole fraction in the critical nucleus:

$$\begin{aligned} X_{al} &= D + E \ln N_{av} \\ D &= 1.2233 - \frac{0.0154RA}{RA + RH} - 0.0415 \ln N_{wv} + 0.0016T. \\ E &= 0.0102 \end{aligned}$$

$N_{av}$ and $N_{wv}$ are the sulphuric acid and water vapor concentrations (cm$^{-3}$) and *RA* denotes relative acidity. After some mathematical manipulation, the change rate in mass mixing ratio for $H_2SO_4$ vapor due to nucleation can be expressed as:

$$\frac{\partial \chi_{H_2SO_4}}{\partial t} = -C_1 \chi_{H_2SO_4}^{C_2}. \tag{A13}$$

where

$$\begin{aligned} C_2 &= A + BE \\ C_1 &= \left( \frac{1}{N_{ac}} \right)^A \left( \frac{6.023 \times 10^{23} \rho_a}{98.1 \times 10^3} \right)^{C_2} \frac{\exp(BD + C)}{\rho_a} 4.189 \cdot \bar{r}_0^3 \rho_d \times 10^6 \end{aligned}$$

[57] Condensation rate of $H_2SO_4$(g) to an existing aerosol particle is described using modified Fuchs-Sutugin equation [*Fuchs and Sutugin*, 1971]

$$J_{cond} = 4\pi D r_i F(Kn) A (P - P_0) \tag{A14}$$

where $r_i$ is the radius in size bin $i$, $Kn$ is the Knudsen number and $D$ is the diffusion coefficient of $H_2SO_4$(g) in air and $F(Kn)$ is a coefficient correcting for free molecular effects,

$$F(Kn) = \frac{1 + Kn}{1 + 1.71Kn + 1.33Kn^2}$$

and $A$ is a coefficient correcting for the interfacial mass transport limitations described by the accommodation coefficient $a_e$.

$$A = \left[1 + 1.33KnF(Kn)\left(\frac{1}{a_e} - 1\right)\right]^{-1}$$

The $P$ and $P_0$ are the vapor pressure of $H_2SO_4$ in the gas phase and its partial pressure at the particle surface, respectively. Usually $P_0$ is quite small ($\sim 10^{-5}$ ppt) and can be assumed to be zero. The total condensation rate to a size bin is expressed as:

$$\frac{\partial \chi_{H_2SO_4}}{\partial t} = -C_3 \chi_{H_2SO_4} \tag{A15}$$

where

$$C_3 = 4\pi D r_i F(Kn) A \cdot R \cdot T \cdot N_i$$

[58] **Acknowledgments.** The authors wish to thank the Canadian Climate Research Network (CCRN) and Program on Energy Research and Development (PERD) for their financial supports for this research. The global land use data are distributed by the EROS Data Center Distributed Active Archive Center (EDC DAAC), located at the U.S. Geological Survey's EROS Data Center in Sioux Falls, South Dakota.

## References

Ackermann, I. J., H. Hass, M. Memmesheimer, A. Ebel, F. S. Binkowski, and U. Shankar, Modal Aerosol Dynamics model for Europe: Development and first applications, *Atmos. Environ.*, *32*, 2981–2999, 1998.

Adams, P. J., J. H. Seinfeld, D. Koch, L. Mickley, and D. Jacob, General circulation model assessment of direct radiative forcing by the sulfate-nitrate-ammonium-water inorganic aerosol system, *J. Geophys. Res.*, *106*, 1097–1111, 2001.

Arakawa, A., and W. H. Schubert, Interaction of a Cumulus Cloud Ensemble with the Large-Scale Envrionment, Part I, *J. Atmos. Sci.*, *31*, 674–701, 1974.

Atkinson, R., D. L. Baulch, R. A. Cox, J. R. F. Hampson, J. A. Derr, and J. Troe, Evaluated kinetics and photochemical data for atmospheric chemistry: Supplement III, *J. Phys. Chem. Ref. Data*, *88*, 881–1097, 1989.

Barrie, L. A., et al., A Comparison of large scale atmospheric sulphate aerosol models (COSAM): Overview and highlights, *Tellus, Ser. B*, *53*, 615–645, 2001.

Beheng, K. D., A parameterization of warm cloud microphysical conversion processes, *Atmos. Res.*, *33*, 193–206, 1994.

Binkowski, F. S., The aerosol portion of Models-3 CMAQ, section 5.6 of draft, Models-3 CMAQ Sci. Doc., U.S. Environ. Prot. Agency, Research Triangle Park, N. C., 1998.

Binkowski, F. S., and U. Shankar, The Regional Particulate Matter Model, 1, Model description and preliminary results, *J. Geophys. Res.*, *100*, 26,191–26,209, 1995.

Brasseur, G. P., D. A. Hauglustaine, S. Walters, P. J. Rasch, J.-F. Müller, C. Granier, and X. X. Tie, MOZART, a global chemical transport model for ozone and related chemical tracers, 1, Model description, *J. Geophys. Res.*, *103*, 28,265–28,289, 1998.

Brook, R. D., J. R. Brook, B. Urch, R. Vincent, S. Rajagopalan, and F. S. Silverman, Inhalation of fine particulate air pollution and ozone causes acute arterial vasoconstriction in healthy adults, *Circulation*, *105*, 1534–1536, 2002.

Burnett, R. T., S. Cakmak, J. R. Brook, and D. Krewski, The role of particulate size and chemistry in the association between summertime ambient air pollution and hospitalization for cardio-respiratory diseases, *Environ. Health Perspect.*, *105*, 614–620, 1997.

Charlson, R. J., and J. Heintzenberg, Aerosol forcing of climate, in *Environmental Sciences Research Report*, pp. 11–108, John Wiley, New York, 1995.

Chin, M., D. J. Jacob, G. M. Gardner, and P. A. Spiro, A global three-dimensional model of tropospheric sulfate, *J. Geophys. Res.*, *101*, 18,667–18,690, 1996.

Cohen, M. D., R. C. Flagan, and J. H. Seinfeld, Studies of concentrated electrolyte solutions using the eletrodynamic balance, 1, Water activities for single-electrolyte solutions, *J. Phys. Chem.*, *91*, 4563–4574, 1987a.

Cohen, M. D., R. C. Flagan, and J. H. Seinfeld, Studies of concentrated electrolyte solutions using the eletrodynamic balance, 2, Water activities for mixed-electrolyte solutions, *J. Phys. Chem.*, *91*, 4575–4582, 1987b.

DeMore, W. B., S. P. Sander, D. M. Golden, R. F. Hampson, C. J. Howard, A. R. Ravishankara, C. E. Kolb, and M. H. Molina, Chemical kinetics and photochemical data for use in stratospheric modeling, *JPL Publ., 92-20*, 1992.

Erickson, D. J., III, J. J. Walton, S. J. Ghan, and J. E. Penner, Three-dimensional modeling of the global atmospheric sulfur cycle: A first step, *Atmos. Environ., Part A*, *25*, 2513–2520, 1992.

Fuchs, N. A., and A. G. Sutugin, Highly dispersed aerosols, in *Topics in Current Aerosol Research*, edited by G. M. Hidy and J. R. Brock, pp. 1–60, Pergamon, New York, 1971.

Gerber, H. E., Relative-humidity parameterization of the Navy Aerosol Model (NAM), report, Nav. Res. Lab., Washington, D. C., 1985.

Ghan, S. J., C. C. Chuang, and J. E. Penner, A parameterization of cloud droplet nucleation, part I, Single aerosol type, *Atmos. Res.*, *30*, 197–221, 1993.

Ghan, S. J., C. C. Chuang, R. C. Easter, and J. E. Penner, A parameterization of cloud droplet nucleation, part II, Multiple aerosol types, *Atmos. Res.*, *36*, 39–54, 1995.

Ghan, S., R. Easter, J. Hudson, and F.-M. Breon, Evaluation of aerosol indirect radiative forcing in MIRAGE, *J. Geophys. Res.*, *106*, 5317–5334, 2001a.

Ghan, S., N. Laulainen, R. Easter, R. Wagener, S. Nemesure, E. Chapman, Y. Zhang, and R. Leung, Evaluation of aerosol direct radiative forcing in MIRAGE, *J. Geophys. Res.*, *106*, 5295–5316, 2001b.

Ghan, S. J., R. C. Easter, E. G. Chapman, H. Abdul-Razzak, Y. Zhang, L. R. Leung, N. S. Laulainen, R. D. Saylor, and R. A. Zaveri, A physically based estimate of radiative forcing by anthropogenic sulfate aerosol, *J. Geophys. Res.*, *106*, 5279–5293, 2001c.

Ginoux, P., M. Chin, I. Tegen, J. Prospero, B. N. Holben, O. Dubovik, and S.-J. Lin, Sources and distributions of dust aerosols simulated with the GOCART model, *J. Geophys. Res.*, *106*, 20,255–20,274, 2001.

Giorgi, F., and W. L. Chameides, Rainout lifetimes of highly soluble aerosols and gases as inferred from simulations with a general circulation model, *J. Geophys. Res.*, *91*, 14,367–14,376, 1986.

Gong, S. L., L. A. Barrie, and J.-P. Blanchet, Modeling sea-salt aerosols in the atmosphere, 1, Model development, *J. Geophys. Res.*, *102*, 3805–3818, 1997.

Gong, S. L., L. B. Barrie, and M. Lazare, Canadian Aerosol Module: A size-segregated simulation of atmospheric aerosol processes for climate and air quality models, 2, Global sea-salt aerosol and its budgets, *J. Geophys. Res.*, *107*, doi:10.1029/2001JD002004, in press, 2002.

Graf, H.-F., J. Feichter, and B. Langmann, Volcanic sulfer emissions: Estimates of source strength and its contribution to the global sulfate distribution, *J. Geophys. Res.*, *102*, 10,727–10,738, 1997.

Greenfield, S., Rain scavenging of radioactive particulate matter from the atmosphere, *J. Meteorol.*, *14*, 115–125, 1957.

Gultepe, I., and G. A. Isaac, The relationship between cloud droplet and aerosol number concentrations for climate models, *Int. J. Climatol.*, *16*, 941–946, 1996.

Hänel, G., The properties of atmospheric aerosol particles as functions of the relative humidity at thermodynamic equilibrium with the surrounding moist air, *Adv. Geophys.*, *19*, 73–188, 1976.

Hauglustaine, D. A., G. P. Brasseur, S. Walters, P. J. Rasch, J.-F. Müller, L. K. Emmons, and M. A. Carroll, MOZART, a global chemical transport model for ozone and related chemical tracers, 2, Model results and evaluation, *J. Geophys. Res.*, *103*, 28,291–28,335, 1998.

Herbert, F., and K. D. Beheng, Scavenging of airborne particles by collision with water drops—Model studies on the combined effect of essential microdynamic mechanisms, *Meteorol. Atmos. Phys.*, *35*, 201–211, 1986.

Intergovernmental Panel on Climate Change (IPCC), *Climate Change 2001: The Scientific Basis, Contribution of Working Group I to the Third Assessment Report of the Intergovernmental Panel on Climate Change*, Cambridge Univ. Press, New York, 2001.

Jacobson, M. Z., Developing, coupling and applying a gas, aerosol, transport and radiation model to study urban and regional air pollution, Ph.D. thesis, Univ. of Calif., Los Angeles, 1994.

Jacobson, M. Z., Development and application of a new air pollution modeling system, part II, Aerosol module structure and design, *Atmos. Environ.*, *31*, 131–144, 1997a.

Jacobson, M. Z., Development and application of a new air pollution modeling system, part III, Aerosol-phase simulations, *Atmos. Environ.*, *31*, 587–608, 1997b.

Jacobson, M. Z., GATOR-GCMM: A global- through urban-scale air pollution and weather forecast model, part 1, Model design and treatment of

subgrid soil, vegetation, roads, rooftops, water, sea ice, and snow, *J. Geophys. Res.*, *106*, 5385–5401, 2001.
Jacobson, M. Z., R. P. Turco, E. J. Jensen, and O. B. Toon, Modeling coagulation among particles of different composition and size, *Atmos. Environ.*, *28*(7), 1327–1338, 1994.
Jacobson, M. Z., R. Lu, R. P. Turco, and O. B. Toon, Development and application of a new air pollution modeling system, part I, Gas-phase simulations, *Atmos. Environ.*, *30*, 1939–1963, 1996.
Jones, A., D. L. Roberts, and J. Slingo, A climate model study of indirect radiative forcing by anthropogenic sulphate aerosols, *Nature*, *370*, 450–453, 1994.
Koloutsou-Vakakis, S., M. J. Rood, A. Nenes, and C. Pilinis, Modeling of aerosol properties related to direct climate forcing, *J. Geophys. Res.*, *103*, 17,009–17,032, 1998.
Kulmala, M., A. Laaksonen, and L. Pirjola, Parameterizations for sulfuric acid/water nucleation rates, *J. Geophys. Res.*, *103*, 8301–8307, 1998.
Leaitch, W. R., G. A. Isaac, J. W. Strapp, C. M. Banic, and H. A. Wiebe, The relationship between cloud droplet number concentrations and anthropogenic pollution: Observation and climatic implications, *J. Geophy. Res.*, *97*, 2463–2474, 1992.
Liousse, C., J. E. Penner, C. Chuang, J. J. Walton, H. Eddleman, and H. Cachier, A global three-dimensional model study of carbonaceous aerosols, *J. Geophys. Res.*, *101*, 19,411–19,432, 1996.
Lohmann, U., and J. Feichter, Impact of sulfate aerosols on albedo and lifetime of clouds: A sensitivity study with the ECHAM4 GCM, *J. Geophys. Res.*, *102*, 13,685–13,700, 1997.
Lohmann, U., and E. Roeckner, Design and performance of a new cloud micro-physics scheme developed for the ECHAM general circulation model, *Clim. Dyn.*, *12*, 557–572, 1996.
Lohmann, U., J. Feichter, C. Chuang, and J. Penner, Predicting the number of cloud droplets in the ECHAM GCM, *J. Geophys. Res.*, *104*, 9169–9198, 1999.
Martin, G. M., D. W. Johnson, and A. Spice, The measurement and parameterization of effective radius of droplets in worm stratocumulus clouds, *J. Atmos. Sci.*, *51*, 1823–1842, 1994.
Meng, Z., D. Dabdub, and J. H. Seinfeld, Chemical coupling between atmospheric ozone and particulate matter, *Science*, *277*, 116–119, 1997.
Meng, Z., D. Dabdub, and J. H. Seinfeld, Size-resolved and chemically resolved model of atmospheric aerosol dynamics, *J. Geophys. Res.*, *103*, 3419–3435, 1998.
Nenes, A., S. N. Pandis, and C. Pilinis, Continued development and testing of a new thermodynamic aerosol module for urban and regional air quality models, *Atmos. Environ.*, *33*(10), 1553–1560, 1999.
O'Dowd, C. D., J. Lowe, M. H. Smith, and A. D. Kaye, The relative importance of sea-salt and nss-sulphate aerosol to the marine CCN population: An improved multi-component aerosol-droplet parameterisation, *Q. J. R. Meteorol. Soc., Part B*, *125*, 1295–1313, 1999.
Padro, J., H. H. Neumann, and G. D. Hartog, An investigation of the ADOM dry deposition module using summertime $O_3$ measurements above a deciduous forest, *Atmos. Environ., Part A*, *25*, 1689–1704, 1991.
Penner, J. E., R. E. Dickinson, and C. A. O'Neill, Effects of aerosol from biomass burning on the global radiation budget, *Science*, *256*, 1432–1433, 1992.
Pham, M., J.-F. Müller, G. P. Brasseur, C. Granier, and G. Mégie, A three-dimensional study of the tropospheric sulfur cycle, *J. Geophys. Res.*, *100*, 26,061–26,092, 1995.
Pilat, M. J., Collection of aerosol particles by electrostatic drop spray scrubbers, *J. Air Pollut. Control Assoc.*, *25*, 176–178, 1975.
Pruppacher, H. R., and J. D. Klett, *Microphysics of Clouds and Precipitation*, 714 pp., Kluwer Acad., Norwell, Mass., 1997.
Quinn, P. K., et al., Surface submicron aerosol chemical composition: What fraction is not sulfate?, *J. Geophys. Res.*, *105*, 6785–6805, 1999.
Raes, F., A. Saltelli, and R. V. Dingenen, Modelling formation and growth of $H_2SO_4$-$H_2O$ aerosols: Uncertainty analysis and experimental evaluation, *J. Aerosol Sci.*, *23*, 757–771, 1992.
Roelofs, G. J., J. Lelieveld, and L. Ganzeveld, Simulation of global sulfate distribution and the influence on effective cloud drop radii with a coupled photochemistry sulfur cycle model, *Tellus, Ser. B*, *50*, 224–242, 1998.
Samet, J., F. Dominici, and F. E. A. Curriero, Fine particulate air pollution and mortality in 20 U.S. cities, *N. Engl. J. Med.*, *343*, 1742–1749, 2000.
Sangster, J., T. T. Tang, and F. Lenzi, A general method of calculating the water activity of supersaturated aqueous solutions from ternary data, *Can. J. Chem. Eng.*, *51*, 2626–2631, 1973.
Saxena, P., and T. W. Peterson, Thermodynamics of multicomponent electrolytic aerosols, *J. Colloid Interface Sci.*, *79*, 496–510, 1981.
Seinfeld, J. H., and S. N. Pandis, *Atmospheric Chemistry and Physics: From Air Pollution to Climate Change*, 1326 pp., John Wiley, New York, 1998.
Slinn, W. G. N., Precipitation scavenging, in *Atmospheric Science and Power Production*, edited by D. Randerson, *Doc. DOE/TIC-27601*, pp. 466–532, Tech. Inf. Cent., Off. of Sci. and Tech. Inf., U.S. Dep. of Energy, Washington, D. C., 1984.
Stokes, R. H., and R. A. Robinson, Interactions in aqueous nonelectrolyte solution, I, Solute-solvent equilibria, *J. Phys. Chem.*, *70*, 2126–2130, 1966.
Tang, I. N., Chemical and size effects of hygroscopic aerosols on light scattering coefficients, *J. Geophys. Res.*, *101*, 19,245–19,250, 1996.
Tang, I. N., and H. R. Munkelwitz, Water activities, densities, and refractive indices of aqueous sulfates and sodium nitrate droplets of atmospheric importance, *J. Geophys. Res.*, *99*, 18,801–18,808, 1994.
Tang, I. N., A. C. Tridico, and K. H. Fung, Thermodynamic and optical properties of sea salt aerosols, *J. Geophys. Res.*, *102*, 23,269–23,277, 1997.
Tegen, I., and I. Fung, Modeling of mineral dust in the atmosphere: Sources, transport, and optical thickness, *J. Geophys. Res.*, *99*, 22,897–22,914, 1994.
Tegen, I., and I. Fung, Contribution the atmospheric mineral aerosol load from land surface modification, *J. Geophys. Res.*, *101*, 19,237–19,245, 1996.
Tegen, I., P. Hollrig, C. Chin, I. Fung, J. Daniel, and J. Penner, Contribution of different aerosol species to the global aerosol extinction optical thickness: Estimates from model results, *J. Geophys. Res.*, *102*, 23,895–23,915, 1997.
Tremmel, H. G., W. Junkermann, and F. Slemr, On the distribution of hydrogen peroxide in the lower troposphere over the northeastern United States during late summer 1988, *J. Geophys. Res.*, *98*, 1083–1099, 1993.
Vedal, S., Ambient particles and health: Lines that divide, *J. Air Waste Manage. Assoc.*, *47*, 551–581, 1997.
von Salzen, K., H. G. Leifhton, P. A. Ariya, L. A. Barrie, S. L. Gong, J.-P. Blanchet, L. Spacek, U. Lohmann, and L. I. Kleinman, Sensitivity of sulphate aerosol size distribution and CCN concentration over North America to $SO_x$ emissions and $H_2O_2$ concentrations, *J. Geophys. Res.*, *105*, 9741–9766, 2000.
Wexler, A. S., F. W. Lurmann, and J. H. Seinfeld, Modelling urban and regional aerosols, I, Model development, *Atmos. Environ.*, *28*, 531–546, 1994.
Whitby, E. R., and P. H. McMurry, Modal aerosol dynamics modeling, *Aerosol Sci. Technol*, *27*, 673–688, 1997.
Zhang, G. J., and N. A. McFarlane, Sensitivity of climate simulations to the parameterization of cumulus convection in the Canadian Climate Centre General Circulation Model, *Atmos. Ocean*, *33*, 407–446, 1995.
Zhang, L., S.-L. Gong, J. Padro, and L. Barrie, A size-segregated particle dry deposition scheme for an atmospheric aerosol module, *Atmos. Environ.*, *35*(3), 549–560, 2001.

L. A. Barrie, Environment Division, Atmospheric Research and Environment Program, World Meteorological Organization, 7 bis, avenue de la Paix, CH-1211 Geneva 2, Switzerland.

J.-P. Blanchet, E. Girard, and L. Spacek, Earth Sciences Department, University of Quebec at Montreal, P.O. Box 8888, Station "Centre Ville," 201 President Kennedy Ave., Montreal, Quebec, Canada H3C 3P8.

P. Chylek, G. Lesins, and U. Lohmann, Atmospheric Science Program, Department of Physics, Dalhousie University, Halifax, Nova Scotia, Canada B3H 3J5.

S. L. Gong, P. Huang, R. Leaitch, H. Lin, and L. M. Zhang, Meteorological Service of Canada, 4905 Dufferin Street, Downsview, Ontario, Canada M3H 5T4. (sunling.gong@ec.gc.ca)

H. Leighton and K. von Salzen, Department of Atmospheric and Oceanic Sciences, McGill University, 805 Sherbrooke St. W., Montreal, Quebec, Canada H3A 2K6.